

This discussion paper is/has been under review for the journal Atmospheric Chemistry and Physics (ACP). Please refer to the corresponding final paper in ACP if available.

Validation of the Swiss methane emission inventory by atmospheric observations and inverse modelling

S. Henne¹, D. Brunner¹, B. Oney¹, M. Leuenberger², W. Eugster³,
I. Bamberger^{3,4}, F. Meinhardt⁵, M. Steinbacher¹, and L. Emmenegger¹

¹Empa Swiss Federal Laboratories for Materials Science and Technology,
Überlandstrasse 129, Dübendorf, Switzerland

²Univ. of Bern, Physics Inst., Climate and Environmental Division, and Oeschger Centre for
Climate Change Research, Bern, Switzerland

³ETH Zurich, Inst. of Agricultural Sciences, Zurich, Switzerland

⁴Institute of Meteorology and Climate Research Atmospheric Environmental Research
(IMK-IFU), Karlsruhe Institute of Technology (KIT), Garmisch-Partenkirchen, Germany

⁵Umweltbundesamt (UBA), Kirchzarten, Germany

Received: 30 October 2015 – Accepted: 2 December 2015 – Published: 16 December 2015

Correspondence to: S. Henne (stephan.henne@empa.ch)

Published by Copernicus Publications on behalf of the European Geosciences Union.

Title Page

Abstract

Introduction

Conclusions

References

Tables

Figures



Back

Close

Full Screen / Esc

Printer-friendly Version

Interactive Discussion



Abstract

Atmospheric inverse modelling has the potential to provide observation-based estimates of greenhouse gas emissions at the country scale, thereby allowing for an independent validation of national emission inventories. Here, we present a regional scale inverse modelling study to quantify the emissions of methane (CH_4) from Switzerland, making use of the newly established CarboCount-CH measurement network and a high resolution Lagrangian transport model. Overall we estimate national CH_4 emissions to be $196 \pm 18 \text{ Ggyr}^{-1}$ for the year 2013 (1σ uncertainty). This result is in close agreement with the recently revised “bottom-up” estimate of $206 \pm 33 \text{ Ggyr}^{-1}$ published by the Swiss Federal Office for the Environment as part of the Swiss Greenhouse Gas Inventory (SGHGI). Results from sensitivity inversions using alternative prior emissions, covariance settings, baseline treatments, two different inverse algorithms (Bayesian and extended Kalman Filter), and two different transport models confirms the robustness and independent character of our estimate. According to the latest “bottom-up” inventory the main CH_4 source categories in Switzerland are agriculture (78%), waste handling (15%) and natural gas distribution and combustion (6%). The spatial distribution and seasonal variability of our posterior emissions suggest an overestimation of agricultural CH_4 emissions by 10 to 20% in the most recent national inventory, which is likely due to an overestimation of emissions from manure handling. Urban areas do not appear as emission hotspots in our posterior results suggesting that leakages from natural gas distribution are only a minor source of CH_4 in Switzerland. This is consistent with rather low emissions of 8.4 Ggyr^{-1} reported by the SGHGI but inconsistent with the much higher value of 32 Ggyr^{-1} implied by the EDGARv4.2 inventory for this sector. Increased CH_4 emissions (up to 30% compared to the prior) were deduced for the north-eastern parts of Switzerland. This feature was common to most sensitivity inversions, which rules out an artefact of the transport model and the inversion system. However, it was not possible to assign an unambiguous source process to the region. The observations of the CarboCount-CH network provided invaluable and independent

Swiss methane emissions

S. Henne et al.

Title Page

Abstract

Introduction

Conclusions

References

Tables

Figures



Back

Close

Full Screen / Esc

Printer-friendly Version

Interactive Discussion



information for the validation of the national bottom-up inventory. Similar systems need to be sustained to provide independent monitoring of future climate agreements.

1 Introduction

Atmospheric methane (CH_4) acts as an important greenhouse gas (GHG) whose man-made increase from pre-industrial to present day levels (from $\approx 700 \text{ nmol mol}^{-1}$ in 1750 to $1819 \text{ nmol mol}^{-1}$ in 2012) directly and indirectly contributes 0.97 ($0.74\text{--}1.20$) W m^{-2} to present day global radiative forcing (Myhre et al., 2013). As such, its contribution to human-induced global warming is second only to carbon dioxide (CO_2). Globally, natural sources (wetlands, lakes, geological seeps, termites, methane hydrates, and wild animals) and anthropogenic sources (fossil fuel extraction, distribution and combustion, rice cultivation, ruminants, and waste) each contribute about half to CH_4 emissions to the atmosphere (Kirschke et al., 2013), but larger uncertainties are connected with the natural sources. Owing to increased research efforts in recent years, uncertainties associated with these fluxes have decreased on the global and continental scale (Kirschke et al., 2013, and references therein). However, there remain open questions about the contributing processes and their temporal and spatial distributions on the regional scale (Nisbet et al., 2014).

In many developed countries natural CH_4 sources are of limited importance (Bergamaschi et al., 2010) and anthropogenic emissions dominate. For example $\approx 98\%$ of Swiss CH_4 emissions are thought to be of anthropogenic origin (Hiller et al., 2014a). Owing to its comparatively short atmospheric lifetime (≈ 10 years) CH_4 has been classified as a short-lived climate pollutant, and reducing anthropogenic CH_4 emissions has become a promising target to lower near-term radiative forcing (Ramanathan and Xu, 2010; Shindell et al., 2012). However, the development of efficient mitigation strategies requires detailed knowledge of the source processes and the success of the mitigation measures should be monitored once put into action. The Kyoto protocol sets legally binding GHG emission reduction targets for Annex-1 countries and the United Nations

Swiss methane emissions

S. Henne et al.

Title Page

Abstract

Introduction

Conclusions

References

Tables

Figures



Back

Close

Full Screen / Esc

Printer-friendly Version

Interactive Discussion



Framework Convention on Climate Change (UNFCCC) calls signatory countries to report their annual GHG emissions of CO₂, CH₄, nitrous oxide, sulphur hexafluoride, and halocarbons.

In Switzerland, the Federal Office for the Environment (FOEN) collects activity data and emission factors in the Swiss Greenhouse Gas Inventory (SGHGI) (FOEN, 2014, 2015) and annually reports emissions following IPCC guidelines (IPCC, 2006). According to this inventory, emissions from agriculture are the single most important source (161.5 Ggyr⁻¹) in Switzerland, followed by waste handling (32.3 Ggyr⁻¹) and fossil fuel distribution and combustion (12.1 Ggyr⁻¹, all values refer to the 2015 reporting for the year 2012). Estimates following IPCC guidelines are derived bottom-up from source-specific information combined with activity data and other statistical data, all of which may contain considerable uncertainties. Methane emissions from individual sources are much more difficult to quantify than anthropogenic emissions of CO₂. As a consequence, the uncertainty assigned to total Swiss CH₄ emissions ($\pm 16\%$) is much larger than that of CO₂ emissions ($\pm 3\%$) (FOEN, 2015). According to the SGHGI, Swiss CH₄ emissions have decreased by about 20% since 1990 (FOEN, 2015), but given the above uncertainties, these estimates require further validation, also in order to survey the effectiveness of the realised reduction measures. Furthermore, considerable differences exist between the SGHGI and other global and European scale inventories (e.g. EDGAR) both in terms of total amount and spatial distribution (Hiller et al., 2014a). Previous validation efforts of the Swiss CH₄ inventory were restricted to flux measurements either on the site scale focusing on a specific emission process (Eugster et al., 2011; Tuzson et al., 2010; Schroth et al., 2012; Schubert et al., 2012) or campaign based flight missions (Hiller et al., 2014b) and tethered balloon soundings (Stieger et al., 2015), mainly confirming estimates of the SGHGI on the local scale. In addition, mobile near-surface measurements were used to verify emission hot spots in a qualitative way (Bamberger et al., 2014). However, it is very difficult to upscale the results of these studies to validate national annual emissions.

Swiss methane emissions

S. Henne et al.

Title Page

Abstract

Introduction

Conclusions

References

Tables

Figures



Back

Close

Full Screen / Esc

Printer-friendly Version

Interactive Discussion



Swiss methane emissions

S. Henne et al.

Title Page

Abstract

Introduction

Conclusions

References

Tables

Figures



Back

Close

Full Screen / Esc

Printer-friendly Version

Interactive Discussion



Such an independent validation of spatially resolved national inventory data can be achieved through inverse modelling yielding a top-down estimate that combines atmospheric observations of the target species with transport modelling and an optimal estimation of the underlying emissions (Enting, 2002; Bergamaschi et al., 2005). Early inverse modelling studies of CH₄ focused on the global scale budget and relied on global flask sampling observations (e.g. Hein et al., 1997; Houweling et al., 1999; Bergamaschi et al., 2000; Dentener et al., 2003; Mikaloff Fletcher et al., 2004). Later studies also included continuous surface and airborne observations (e.g. Vermeulen et al., 1999; Bergamaschi et al., 2005, 2010; Chen and Prinn, 2006; Kort et al., 2010; Manning et al., 2011; Miller et al., 2013) and provide country specific emissions. For data sparse regions, the additional use of satellite retrieved CH₄ data in atmospheric inversions has recently helped reducing uncertainties (Meirink et al., 2008; Bergamaschi et al., 2013) and increased the ability to deduce emissions with higher spatial resolution (Wecht et al., 2014; Turner et al., 2015). However, such top-down estimates were usually not made for small countries and regions like Switzerland (O(10 000 km²)), owing to the coarse spatial resolution of the inversion systems. Recent studies from the USA have shown large differences between national and regional bottom-up estimates and inverse modelling, predominantly detecting large emission underestimations in the bottom-up inventories (Wecht et al., 2014; Turner et al., 2015; Miller et al., 2013; McKain et al., 2015; Wennberg et al., 2012). These were mainly attributed to three major source processes: oil and gas extraction, ruminants, and natural gas distribution to the end user.

Here, we validate the bottom-up estimate of Swiss CH₄ emissions as given in the SGHGI by analysing continuous, near surface observations of CH₄ from the newly established, dense CarboCount-CH measurement network in central Switzerland (Oney et al., 2015) and two neighbouring sites. For the first time, we apply an inverse modelling framework with high spatial resolution to a relatively small area with considerable land surface heterogeneity and topographical complexity. Such modelling approaches have only recently become feasible through the use of high-resolution atmospheric

transport simulations (e.g. for CH₄, McKain et al., 2015). The main aim of the study is to provide an independent validation of the SGHGI in terms of national total emissions (FOEN, 2015), geographical (Hiller et al., 2014a) and temporal distribution. Results in the spatio-temporal distribution shall be used to draw conclusions on the estimates of individual source processes.

2 Data and methods

2.1 Observations

The CH₄ observations used in this study are those of the CarboCount-CH¹ network (BEO, LAE, FRU, GIM) located on the Swiss Plateau and those from two additional mountain sites: Jungfrauoch and Schauinsland (see Fig. 1, S1 in the Supplement and Table 1). The Swiss Plateau, the relatively flat area between the Alps in the south and Jura mountains in the north, covers only about one third of the area of Switzerland but is home to two thirds of the Swiss population and is characterized by intensive agriculture and extended urban and suburban areas. Approximately two thirds of the Swiss CH₄ emissions are thought to stem from this area (Hiller et al., 2014a). Oney et al. (2015) characterised the transport to the CarboCount-CH sites applying the same transport model as used here. They find that all four sites are mainly sensitive to emissions from most of the Swiss Plateau during summer day-time conditions, whereas sensitivities are more localised around the sites in winter, but still provide reasonable coverage of the targeted area of the Swiss Plateau.

The Beromünster (BEO) site is located on a hill in an intensively used agricultural area. It is surrounded mainly by croplands and to a smaller extent rangeland. The site itself consists of a 217 m high decommissioned radio transmission tower. Gas inlets and meteorological instrumentation are installed on the tower at 5 different heights above ground (12 to 212 m), whereas the gas analyser is located at the foot of the

¹<http://www.carbocount.ch>, last accessed 9 September 2015

Swiss methane emissions

S. Henne et al.

Title Page

Abstract

Introduction

Conclusions

References

Tables

Figures

◀

▶

◀

▶

Back

Close

Full Screen / Esc

Printer-friendly Version

Interactive Discussion



Swiss methane emissions

S. Henne et al.

Title Page

Abstract

Introduction

Conclusions

References

Tables

Figures



Back

Close

Full Screen / Esc

Printer-friendly Version

Interactive Discussion



tower. A comprehensive description of the installation and the measurement system can be found in Berhanu et al. (2015). Here, only the observations from the topmost inlet height (212 m) were used, since this height showed the largest extent of the relative footprint and, hence, is least influenced by local sources (Oney et al., 2015).

Lägern Hochwacht (LAE) is a mountain top site on a a very steep, west–east extending crest approximately 15 km north-west of and 400 m above the city centre of Zurich, the largest city in Switzerland. The site is surrounded by forest with average tree crown heights of 20 m close to the site. The gas inlet and meteorological instrumentation is mounted on a small tower of 32 m.

Frübüel (FRU) is another mountain site and located at 982 m a.s.l. above lake Zug on the south-eastern edge of the Swiss Plateau. Unlike Lägern-Hochwacht, the site is located on a mountain top plateau with a south-west aspect above lake Zug and with slightly more elevated areas to the south-east. The area around the site is used as rangeland and emissions from a local dairy farm may influence the observations. In contrast to the other sites, gas samples and meteorological observations are taken close to the surface (3 m above ground). A more detailed analysis of how the observations of this site are locally influenced and how they can be compared to observations from the close-by tall tower in BEO is given in Bamberger et al. (2015). Here we only note that the influence of local emissions that cannot be accounted for in the transport model needs to be filtered from the observational data before the use in inverse modelling. We did this by removing all data (10 min resolution) with low wind speeds ($< 3 \text{ m s}^{-1}$) coming from the direction of the aforementioned farm (140 to 200°). These thresholds were determined by comparing differences between the observations of BEO (212 m), which exhibit less local influences, and FRU as a function of wind speed and direction at FRU.

At the Gimmiz site (GIM, 443 m a.s.l.) sample gases are drawn from a 32 m tall water tower. The surrounding area is flat and dominated by intensive agriculture, mostly vegetable farming and croplands. The area is a transformed wetland that used to be regularly flooded until the 1850s before the leveling of the river system (1868–1891)

Swiss methane emissions

S. Henne et al.

Title Page

Abstract

Introduction

Conclusions

References

Tables

Figures



Back

Close

Full Screen / Esc

Printer-friendly Version

Interactive Discussion



when also former wetlands were converted to agricultural lands (Schneider and Eugster, 2007). Although there are only two small farms in the direct vicinity, larger potential CH_4 sources are located in the town of Aarberg about 2.5 km to the south-east. Here a sugar refinery, operating a large-scale waste water treatment plant (250 000 person equivalent), a compost and soil recycling facility, and a biogas reactor for electrical power generation are located. These local sources may not be represented sufficiently well in model simulations. Therefore and as in the case of FRU, observations from GIM were filtered by wind speed and direction, excluding all 10 min averages for which wind speeds were either below 2 m s^{-1} or coming from directions between 90 and 150° . Again these thresholds were estimated by comparison to the observations at BEO.

Schauinsland (SSL, 1205 m a.s.l.) is a mountain top site in the Black Forest, Germany, to the north of the Swiss Plateau. As such it is usually situated above the stable nocturnal boundary layer of the surrounding, but at day-time it is affected by boundary layer air (Schmidt et al., 1996). The site is surrounded by forests and rangeland and no large CH_4 source is known in the direct vicinity. While not part of CarboCount-CH network, the observations from SSL provide additional constraints for the atmospheric inversion especially at mid-distance from the Swiss Plateau.

The high-altitude observatory Jungfraujoch (JFJ, 3580 m a.s.l.) is located in the northern Swiss Alps on a steep mountain saddle between the two mountains Jungfrau (4158 m a.s.l.) and Mönch (4099 m a.s.l.). Although JFJ is usually located in the free troposphere, it intermittently receives polluted boundary layer air both from sources north and south of the Alps (Zellweger et al., 2003; Henne et al., 2010; Tuzson et al., 2011). The intensity of these transport events from the boundary layer can vary strongly depending on the weather condition and the transport process responsible for lifting.

At all sites CH_4 measurements were carried out using PICARRO (Santa Clara, CA, USA) cavity ring-down spectrometers (Rella et al., 2012) which provide high frequency (approximately 0.5 to 1 Hz) observations of CO_2 , CH_4 , H_2O and (at BEO and LAE) CO . All instruments were calibrated against the WMO X2004 CH_4 scale (Dlugokencky et al., 2005) and were reporting dry air mole fractions by either applying a water va-

Swiss methane emissions

S. Henne et al.

Title Page

Abstract

Introduction

Conclusions

References

Tables

Figures



Back

Close

Full Screen / Esc

Printer-friendly Version

Interactive Discussion



por correction accounting for dilution and spectroscopic effects (CarboCount-CH sites and SSL) or by using pre-sample drying of sample air (JFJ). At the CarboCount-CH sites, measurements of additional target gases, not used for the calibration, give an estimate of the instruments' non-random uncertainty for CH_4 of $\approx 0.5 \text{ nmol mol}^{-1}$ (Oney et al., 2015). At SSL observations of three additional target gases yield a combined measurement uncertainty of $0.3 \text{ nmol mol}^{-1}$. For JFJ a combined measurement uncertainty of $\sigma = \sqrt{0.31^2 + (3.61 \times 10^{-4} \times \chi)^2} \text{ nmol mol}^{-1}$ was reported for hourly aggregates, where χ is the observed mole fraction (Empa, 2015).

For the use in the inversion 3 hourly aggregates were produced from high frequency observations for the period 1 March 2013 to 28 February 2014, the first year with a complete set of measurements for all CarboCount-CH sites. Out of the dataset, only the afternoon values, covering 12:00 to 18:00 UTC (CarboCount-CH sites), were used in the atmospheric inversion. This was done in order to capture the time of day with the deepest planetary boundary layer (PBL) extent, which should also be best captured by the transport model and yield the smallest model bias (Kretschmer et al., 2014) and at the same time minimise the influence of local sources and sinks. For the more remote sites JFJ and SSL, the night-time data from 00:00 to 06:00 UTC were used instead, when the sites are least influenced by transport in complex terrain. In addition to the absolute mole fraction, an estimate of the baseline mole fraction, which is supposed to represent conditions without recent emission input, was generated using the “Robust Estimation of Baseline Signal” (REBS) method (Ruckstuhl et al., 2012). The absolute mole fraction of the observations, $\chi_{o, p}$, can then be given as the sum of the baseline, $\chi_{o, b}$, and the contribution due to recent emissions, $\chi_{o, p}$,

$$\chi_{o, p} = \chi_{o, b} + \chi_{o, p} \quad (1)$$

The REBS method iteratively fits a non-parametric local regression curve to the observations, successively excluding points outside a certain range around the baseline curve. REBS was applied separately to hourly data from each site using asymmetric

robustness weights with a tuning factor of $b = 3.5$, a temporal window width of 60 days and a maximum of 10 iterations. An estimate of the baseline uncertainty is given by REBS as a constant value for the whole time series. For JFJ the baseline uncertainty was estimated to $17.4 \text{ nmol mol}^{-1}$, whereas uncertainties for the other sites ranged between $16.2 \text{ nmol mol}^{-1}$ (SSL) and $18.9 \text{ nmol mol}^{-1}$ (LAE), reflecting different degrees of variability and frequency of air masses not influenced by recent surface contact and emissions.

2.2 Transport models

Source sensitivities giving the direct influence of a mass emission from a source location onto the mole fraction at a receptor site were calculated with two different versions of the Lagrangian Particle Dispersion Model (LPDM) FLEXPART (Stohl et al., 2005). The first represents the standard FLEXPART model (version 9.02) driven by analysis fields of the operational runs of the Integrated Forecast System (IFS) of the European Centre for Medium Range Weather Forecast (ECMWF). Input fields were available every 3 h with a horizontal resolution of $0.2^\circ \times 0.2^\circ$ ($\approx 15 \text{ km} \times \approx 22 \text{ km}$) for the Alpine area and $1^\circ \times 1^\circ$ elsewhere. The second FLEXPART version is the one adapted to the use of output from the COSMO regional numerical weather prediction (NWP) model (Baldauf et al., 2011). FLEXPART-COSMO was driven by operational analysis fields as generated hourly by the Swiss national weather service, MeteoSwiss, for Western Europe with a horizontal resolution of approximately $7 \text{ km} \times 7 \text{ km}$. Hourly analysis fields are produced applying an observational nudging technique (Schraff, 1997) to near surface and vertical profile observations of pressure, relative humidity and wind. The use of a high-resolution transport model in regional scale inversions based on point observations is a prerequisite to reduce the representation uncertainty of the model (Tolk et al., 2008; Pillai et al., 2011). Furthermore, the use of a time-inverted LPDM is highly beneficial to this purpose as it allows an accurate transport description in the near-field of the sites below the resolution of the driving meteorology.

Title Page

Abstract

Introduction

Conclusions

References

Tables

Figures



Back

Close

Full Screen / Esc

Printer-friendly Version

Interactive Discussion



Swiss methane emissions

S. Henne et al.

Title Page

Abstract

Introduction

Conclusions

References

Tables

Figures



Back

Close

Full Screen / Esc

Printer-friendly Version

Interactive Discussion



The main differences between FLEXPART-COSMO and standard FLEXPART-ECMWF are the internal vertical grid representation and the parameterisation of convective transport. In FLEXPART-COSMO, the native vertical grid of the COSMO model is used as the main frame of reference, which, in this case, was a height-based hybrid coordinate system (Gal-Chen and Somerville, 1975). In contrast, standard FLEXPART uses a terrain-following vertical coordinate with constant level depths up to the model top, which requires an initial vertical interpolation from the pressure-based hybrid coordinate used in the IFS. In FLEXPART-COSMO, all interpolation to particle positions is done directly from the native COSMO grid, avoiding multiple interpolation errors. In FLEXPART-ECMWF sub-grid scale convection is treated by an Emanuel type scheme (Emanuel and Zivkovic-Rothman, 1999; Forster et al., 2007), whereas in FLEXPART-COSMO the same modified version of the Tiedtke convection scheme (Tiedtke, 1989) as used in COSMO was implemented.

With both model versions source sensitivities were calculated for each observation site and 3 hourly interval. For each interval and location a total of 50 000 particles was released and followed backward in time for 4 and 10 days in the COSMO and ECMWF version, respectively. Particles leaving the limited COSMO-7 domain were terminated prematurely. The limited horizontal model resolution and the complex terrain in the investigated domain lead to differences between the model surface altitude and the real site altitude. In such situations, the most representative height above model ground for particle releases in an LPDM is not well known. Therefore, we chose to release particles at two vertical locations for the CarboCount-CH sites to analyse the sensitivity of this choice. At BEO, where the model topography is relatively close to the site's altitude, these span the possible range of reasonable release altitudes by representing (1) the height above model surface as given by the inlet height of the observations and (2) the absolute altitude above sea level of the inlet. At the sites FRU and LAE the lower release height was chosen 50 m and the higher 150 m above model ground because height deficiencies in the model were larger here. At GIM only one release height was used because the model topography was relatively close to the true surface altitude.

Swiss methane emissions

S. Henne et al.

Title Page

Abstract

Introduction

Conclusions

References

Tables

Figures

◀

▶

◀

▶

Back

Close

Full Screen / Esc

Printer-friendly Version

Interactive Discussion



Also for the more remote sites JFJ and SSL only one release height was simulated that represents the middle between the model surface and the site altitude. Previously it was shown that such an approach works best for the mountaintop site JFJ, which shows large model topography deficits (Brunner et al., 2013). Values for all release heights are given in Table 1.

From both models, output was generated on a regular longitude/latitude grid with a horizontal resolution of $0.16^\circ \times 0.12^\circ$ (≈ 13 km) covering Western Europe and for a nested Alpine domain with a horizontal resolution of $0.02^\circ \times 0.015^\circ$ (≈ 1.7 km). The generated output represents the summed residence time, $\tau_{i,j}$, of particles in a given grid box, i, j , and below a specific sampling height, h_s , divided by the density of dry air in this grid cell and has units $\text{s m}^3 \text{ kg}^{-1} \text{ gridcell}^{-1}$. The sampling height was set to 50 and 100 m above ground in FLEXPART-COSMO and FLEXPART-ECMWF, respectively, coinciding with the minimal PBL height used in the models. Multiplication of $\tau_{i,j}$ with the volume of the sampling grid cell, $V_{i,j} = A_{i,j} \cdot h_s$, and the ratio of the molar weight of the species of interest, μ_s , and the molar weight of dry air, μ_d , yields the desired source sensitivity, $m_{i,j}$, in units $\text{s kg}^{-1} \text{ mol mol}^{-1}$.

$$m_{i,j} = \frac{\tau_{i,j} \mu_d}{V_{i,j} \mu_s}. \quad (2)$$

$m_{i,j}$ provides the effect a mass emission, $E_{i,j}$ (kg s^{-1}), in a source grid box (i, j) would have on the dry air mole fraction at the receptor. The sum over all grid boxes then yields the increase in mole fraction, χ_p , due to recent emissions.

2.3 Inversion framework

In our inversion system the source sensitivities calculated by the transport model can be used to give a direct relationship between the simulated mole fractions and the so called state vector, $\mathbf{x} = (x_1 \dots x_K)$ with a total of K elements, that primarily contains the

desired gridded emissions. In matrix notation this can be expressed as

$$\chi = \mathbf{M}\mathbf{x}, \quad (3)$$

where $\chi = (\chi_1 \dots \chi_L)$ represents the simulated mole fractions at different times and locations, $l = 1, \dots, L$. The sensitivity matrix \mathbf{M} (dimensioned $K \times L$) contains the sensitivities for each time/location towards the k th element of the state vector.

In our case, the state vector contained additional parameters characterising the baseline mole fractions χ_b at different times and for different sites. Hence, \mathbf{x} contained K_E elements describing the emissions and $K_B = K - K_E$ elements giving baseline mole fractions, which were not estimated at each observation but at discrete time intervals (baseline nodes). Therefore, the sensitivity matrix \mathbf{M} consists of two block matrices \mathbf{M}^E and \mathbf{M}^B giving the dependence on the emissions and baseline mole fractions, respectively. Similar to Stohl et al. (2009), elements of \mathbf{M}^B were set to represent temporal linear interpolation between the baseline mole fractions at the neighbouring baseline nodes.

In order to reduce the size of the inversion problem, emissions were not optimised on a regular longitude/latitude grid as given by the FLEXPART simulations. Instead, a reduced grid was used that assigns finer (coarser) grid cells in areas with larger (smaller) average source sensitivities. Starting from the finest output grid resolution of $0.02^\circ \times 0.015^\circ$ grid boxes up to a maximum size of $2.56^\circ \times 1.92^\circ$ were aggregated if their average residence time did not reach a specified threshold. In this way the number of cells in the inversion was reduced to the order of $J_E \approx 1000$. The overall extent of the emission grid was determined by (1) the extent of the COSMO-7 domain, (2) the existence of considerable CH_4 emissions (cut-off over the oceans) and (3) a minimum source sensitivity. Tests with larger and smaller inversion domains did not indicate significant influences on the deduction of Swiss emissions.

In Bayesian atmospheric inversion prior knowledge of the state vector, \mathbf{x}_b , and its probability distribution is used to guide the optimisation process. Mathematically this can be expressed by formulating a cost function J that penalises deviations from the

prior state and differences between simulated and observed mole fractions (e.g. Tarantola, 2005)

$$J = \frac{1}{2}(\mathbf{x} - \mathbf{x}_b)^T \mathbf{B}^{-1} (\mathbf{x} - \mathbf{x}_b) + \frac{1}{2}(\mathbf{M}\mathbf{x} - \boldsymbol{\chi}_o)^T \mathbf{R}^{-1} (\mathbf{M}\mathbf{x} - \boldsymbol{\chi}_o), \quad (4)$$

where \mathbf{x} describes the optimised and \mathbf{x}_b the prior state vector, and $\mathbf{M}\mathbf{x} - \boldsymbol{\chi}_o$ is the difference between simulated and observed mole fractions. \mathbf{B} and \mathbf{R} give the uncertainty covariance matrices of the prior state and the combined model-observation uncertainty. In Sect. 2.4 the structure of these matrices is discussed in more detail. Minimisation of J yields the posterior state

$$\mathbf{x} = \mathbf{x}_b + \mathbf{B}\mathbf{M}^T (\mathbf{M}\mathbf{B}\mathbf{M}^T - \mathbf{R})^{-1} (\boldsymbol{\chi}_o - \mathbf{M}\mathbf{x}_b). \quad (5)$$

In our implementation the inverse of $\mathbf{S} = (\mathbf{M}\mathbf{B}\mathbf{M}^T - \mathbf{R})$, a $L \times L$ matrix, was calculated using LU factorisation (function DGESVX in LAPACK). In addition to the posterior state also its uncertainty expressed as a covariance matrix, \mathbf{A} , can be given (e.g. Tarantola, 2005)

$$\mathbf{A} = \mathbf{B} - \mathbf{B}\mathbf{M}^T \mathbf{S}^{-1} \mathbf{M}\mathbf{B}. \quad (6)$$

The total emissions and their uncertainty from a certain region or country can then be calculated as

$$E = \sum_k^{K_E} x_k f_k; \sigma_E^2 = \mathbf{f}^T \mathbf{A}^E \mathbf{f}, \quad (7)$$

where the vector \mathbf{f} gives the fractional contribution of the region to each inversion grid cell and \mathbf{A}^E is the part of \mathbf{A} that contains the covariance of the posterior emissions. f_k takes a value of 1 for a grid cell that is completely within the region and 0 for grid cells outside the region. For coarse inversion grid cells on the border of a region, f_k was calculated from higher resolution population data, weighting per region contributions by population and not by land surface area.

Swiss methane emissions

S. Henne et al.

Title Page

Abstract

Introduction

Conclusions

References

Tables

Figures

⏪

⏩

◀

▶

Back

Close

Full Screen / Esc

Printer-friendly Version

Interactive Discussion



2.4 Covariance design

This section details the construction of the covariance matrices \mathbf{B} and \mathbf{R} as used in the base inversion. Parameters used to build the matrices were chosen based on experience and previous publications (see below). The sensitivity to these choices was investigated in a set of sensitivity inversions as described in Sect. 2.5.

Both uncertainty covariance matrices are symmetric block matrices. In the case of \mathbf{B} one block, \mathbf{B}^E , describes the uncertainty covariances of the emission vector and a second block, \mathbf{B}^B , the uncertainty covariances of the baseline mole fractions. Within each block the off-diagonal elements were allowed to be non-zero. The diagonal elements of \mathbf{B}^E were set proportional to the prior emissions in the respective grid cell $B_{j,j}^E = (f_E x_{b,j})^2$. For the off-diagonal elements a spatial correlation of the uncertainty was assumed that decays exponentially with the distance between two grid cells

$$B_{i,j}^E = e^{-\frac{d_{i,j}}{L}} \sqrt{B_{i,i}^E} \sqrt{B_{j,j}^E}, \quad (8)$$

where $d_{i,j}$ is the distance between two grid cell centres and L the correlation length. In this setup the total squared uncertainty of the prior emissions $\sigma_E^2 = \mathbf{1}^T \mathbf{B}^E \mathbf{1}$, where $\mathbf{1}$ is a vector of all ones, only depends on the settings of L and f_E . For the base inversion L was fixed to 50 km and f_E was adjusted to yield fixed relative uncertainties of the national estimate for Switzerland.

For the base inversion baseline nodes were spaced equidistantly with a distance of $\tau_B = 5$ days over the observation period and individually for each site, resulting in 73 baseline elements in the state vector for each site. Prior estimates of the baseline mole fractions were REBS estimates for the site JFJ (see Sect. 2.1). All diagonal elements of \mathbf{B}^B were set to a constant value, $B_{i,i}^B = f_b \sigma_b^2$, where σ_b is an estimate of any given baseline uncertainty and f_b is a scaling factor. The off-diagonal elements were set assuming an exponentially decaying correlation of the baseline uncertainty between

Title Page

Abstract

Introduction

Conclusions

References

Tables

Figures

◀

▶

◀

▶

Back

Close

Full Screen / Esc

Printer-friendly Version

Interactive Discussion



baseline nodes

$$B_{i,j}^B = e^{-\frac{T_{i,j}}{\tau_b}} \sqrt{B_{i,i}^B} \sqrt{B_{j,j}^B}, \quad (9)$$

where $T_{i,j}$ is the time difference between two nodes and τ_b is the temporal correlation length. In the base inversion, σ_b was obtained from the REBS fit of the JFJ observations (17.4 nmol mol⁻¹), f_b was set to unity, and τ_b to 14 days.

The block matrix **R** contains one block for each site used in the inversion. In its diagonal elements both the observation and the model uncertainty were considered by quadratic addition

$$R_{i,i} = \sigma_o^2 + \sigma_{\min}^2 + \sigma_{\text{srr}}^2 \chi_{p,i}^2, \quad (10)$$

where σ_o is the observation uncertainty as estimated for each 3 hourly CH₄ average (see Sect. 2.1) and the second and third term are contributions of the model uncertainty. σ_{\min} represents a constant contribution while the third term represents an uncertainty contribution relative to the prior simulation of above baseline concentrations, $\chi_{p,i}$ (Brunner et al., 2012). For the base inversion σ_{\min} and σ_{srr} were estimated separately for each site from the model residuals of the prior simulation $\chi_{p,i}$, by fitting a linear regression through binned RMSEs calculated along $\chi_{p,o}$. Estimating the model uncertainty from the residuals of the prior simulation has been suggested before by Stohl et al. (2009), where σ_{\min} was estimated from all residuals, whereas σ_{srr} was set to 0. In an additional step this constant value was then forced to yield a normal distribution of the normalised model residuals. Furthermore, Stohl et al. (2009) applied their residual estimation in an iterative way using the model residuals from successive inversion runs. In our experience this may lead to underestimated model uncertainties and we did not iterate our procedure. Finally, off-diagonal elements of the model-observations covariance matrix were assumed to follow an exponentially decaying correlation structure.

$$R_{i,j} = e^{-\frac{T_{i,j}}{\tau_o}} \sqrt{R_{i,i}} \sqrt{R_{j,j}}, \quad (11)$$

35432

Swiss methane emissions

S. Henne et al.

Title Page

Abstract

Introduction

Conclusions

References

Tables

Figures

◀

▶

◀

▶

Back

Close

Full Screen / Esc

Printer-friendly Version

Interactive Discussion



Swiss methane
emissions

S. Henne et al.

Title Page

Abstract

Introduction

Conclusions

References

Tables

Figures

◀

▶

◀

▶

Back

Close

Full Screen / Esc

Printer-friendly Version

Interactive Discussion



where $T_{i,j}$ is the time difference between two measurements and τ_o is the temporal correlation length that describes the auto-correlation in the model-observation uncertainty. In the base inversion τ_o was set to 0.5 days, a value previously used by other authors (e.g. Thompson et al., 2011) and associated with the inability of atmospheric transport models to correctly simulate the diurnal cycle in the PBL. The covariances between observations from different sites were set to 0.

2.5 Sensitivity inversions

The Bayesian inversion provides an estimate of the posterior uncertainty of the state vector, which in itself should be sufficient to give an estimate of the combined top-down uncertainty. However, this analytical uncertainty tends to underpredict the true uncertainty. Optimality of the Bayesian approach requires normally distributed probability density functions, uncorrelated residuals, and non-systematic uncertainties, requirements that are difficult to meet exactly in practice. In particular, potential systematic uncertainties in model transport, which may contribute importantly to the overall uncertainty (e.g. Gerbig et al., 2008), are not accounted for. To explore the range of uncertainty beyond the analytically derived posterior uncertainty and to test the robustness of the results to different assumptions, it has therefore been proposed to perform additional sensitivity inversions (e.g. Bergamaschi et al., 2010, 2015). To this end, we set up a series of sensitivity inversions that vary different aspects of the inversion (transport simulations, inversion algorithm, covariance design, prior emissions, observation selection, seasonality of emissions). An overview of these sensitivity inversions is given in Table 2 and details are described in the following.

2.5.1 Transport simulation

One important source of uncertainty when using observational data from elevated sites is the potential mismatch between model and real topography. The choice of the particle release height in the model can considerably change the model's performance and

Swiss methane emissions

S. Henne et al.

Title Page

Abstract

Introduction

Conclusions

References

Tables

Figures



Back

Close

Full Screen / Esc

Printer-friendly Version

Interactive Discussion



may lead to systematic biases in simulated concentrations. Therefore, we quantified the effect of the release height by using a “low” and “high” release case for each of the sensitivity inversions in Table 2. One is always using the lower release heights for the CarboCount-CH stations as introduced in Sect. 2.2, whereas the other uses the higher release heights. The release heights of the more remote sites JFJ and SSL were not varied because of their less direct influence on the Swiss emissions. In addition to the release height, two different versions of the atmospheric transport model were used. The base inversion was based on FLEXPART-COSMO and a sensitivity run used the results of FLEXPART-ECMWF (S-EC).

2.5.2 Seasonal variability

In the base inversion emissions were assumed to be constant in time. To test the implication of this assumption, a sensitivity run extending the state vector to separately hold emissions for each season (S-V) was set up. The number of emission elements in the state vector increased by a factor of four in this case and the sensitivity matrix \mathbf{M} had to be extended accordingly. The prior emissions and their uncertainty were set identical for all seasons. In addition, temporal correlation in the uncertainty covariance matrix of the prior state was treated analogously to the temporal correlation of the observation uncertainty by an exponentially decaying correlation with a time constant of 90 days.

2.5.3 Inversion algorithm

An additional sensitivity test, replacing the Bayesian method by an extended Kalman Filter (extKF) inversion as described in Brunner et al. (2012), was conducted (case S-K). Similar to the Bayesian inversion a prior state vector is used by the extKF. In contrast to the Bayesian approach, the extKF assimilates the observations sequentially from time step to time step. In the extKF approach one baseline value and its tendency for each site are part of the state vector. In each step observations from different sites

Swiss methane emissions

S. Henne et al.

Title Page

Abstract

Introduction

Conclusions

References

Tables

Figures

◀

▶

◀

▶

Back

Close

Full Screen / Esc

Printer-friendly Version

Interactive Discussion



but not from different times are incorporated. This allows for a more flexible temporal evolution of the emissions and the baseline values as for the Bayesian approach. Another important difference is that the extKF method of Brunner et al. (2012) estimates the logarithm of the emissions rather than the emissions themselves to enforce positive fluxes. This renders the problem non-linear and requires the use of an extended Kalman Filter. As in the Bayesian inversion the extKF describes the uncertainties of the prior state and the model-observation uncertainty through the respective covariance matrices **B** and **R**. In addition to these, the extKF requires a covariance matrix **Q** that describes the uncertainty with which the state vector can change from one time step to the next.

2.5.4 Covariance parameters

The next set of sensitivity inversions was designed to analyse the effect of different uncertainty covariance matrices. Our base inversion is based on the prior emission uncertainty as estimated by the bottom-up inventory, which we consider to be the best knowledge of prior uncertainty. Next to the base inversion a set of covariance parameters as estimated by the method of maximum likelihood (ML, Michalak et al., 2005) were used (S-ML). We estimated the covariance parameters (L , f_E , τ_b , and individually for each site f_b , σ_{\min} , σ_{srr}) by minimising the negative logarithm of the likelihood estimator (Michalak et al., 2005)

$$L_\theta = \frac{1}{2} \ln \left| \mathbf{MBM}^T + \mathbf{R} \right| + \frac{1}{2} (\boldsymbol{\chi}_o - \mathbf{M}\boldsymbol{x}_b)^T \left(\mathbf{MBM}^T + \mathbf{R} \right)^{-1} (\boldsymbol{\chi}_o - \mathbf{M}\boldsymbol{x}_b). \quad (12)$$

As a consequence of the ML optimisation posterior model residuals and posterior emission differences should follow a χ^2 distribution. To find the minimum of L_θ a multivariate optimisation routine was used. We applied the Broyden, Fletcher, Goldfarb and Shanno (BFGS) algorithm that is widely used for optimisation problems (see for example Nocedal and Wright, 2006). Initial parameter values were set equal to those used in the base inversion, but giving all sites the same σ_{\min} of 20 nmol mol⁻¹ and σ_{srr} of 1. To as-

sess the robustness of the ML optimisation results an alternative algorithm was tested (Nelder–Mead), yielding very similar parameter sets.

Another sensitivity run varied the design of the model/observation covariance by estimating the diagonal elements of the matrix from the prior RMSE at each site

5 $\sigma_{\min} = \text{RMSE}(\chi_b - \chi_o)$ and applying a correction for extreme residual values according to Stohl et al. (2009) (S-S). Such extreme residuals only occurred for two observations at LAE, so that essentially a constant model uncertainty was used for each site. The off-diagonal elements were calculated in the same way as in the base inversion. For the extKF inversion it was only possible to use a fixed set of parameters σ_{\min} and σ_{SRR} for all sites. They were selected to be close to the average values used in the reference inversion. All covariance parameters used in the base, these two alternative and also the extKF inversion are compared in Table 3. In case of the Bayesian inversions, the covariance parameters differed between the two release heights with the high release showing larger values of σ_{\min} for the sites BEO and LAE and all applied estimation techniques.

2.5.5 Prior emissions

The sensitivity of the inversion result to the prior emissions was tested by using different prior inventories. In our base inversion we used the Swiss MAIOLICA inventory (Hiller et al., 2014a) reflecting the total Swiss emissions for the year 2011 as reported to UNFCCC in 2013. For areas outside Switzerland prior emissions were taken from the European scale inventory developed by TNO for the MACC-2 project (Kuenen et al., 2014) (TNO/MACC-2 hereafter) applying the same country-by-country scaling to 2011 values reported to UNFCCC in 2013. In a sensitivity inversion we replaced the MAIOLICA emissions within Switzerland with those given by TNO/MACC-2 (S-T). A third sensitivity run was set up using the EDGAR (v4.2 FT2000) inventory for the base year 2010 (JRC/PBL, 2009) (S-E). In all three cases the prior uncertainty was set so that a value of $\sigma_E = 16\%$ was reached for the Swiss emissions, which is the uncertainty given for the Swiss bottom-up estimate (FOEN, 2015). For individual grid cells the resulting prior

Swiss methane emissions

S. Henne et al.

Title Page

Abstract

Introduction

Conclusions

References

Tables

Figures



Back

Close

Full Screen / Esc

Printer-friendly Version

Interactive Discussion



uncertainty was $\approx 30\%$. However, the off-diagonal elements in \mathbf{B}^E contributed considerably to the total uncertainty for small grid cells (see Fig. S2 in the Supplement).

2.5.6 Selection of observations

Another series of sensitivity inversions was set up using different parts of the observational data (runs S-01 to S-05, Table 2). The number and combination of sites used in each inversion was varied from using individual sites to using all six sites. For each of these sensitivity cases the inversion grid was adjusted according to the total source sensitivity of the selected sites, thereby assuring that small grid cells only occurred in areas with large sensitivities. In the base inversion the two CarboCount-CH sites BEO and LAE and the two more remote sites JFJ and SSL were used, whereas the observations of FRU and GIM served for validation only.

2.5.7 Baseline treatment

As described above, the baseline mole fractions were treated as a linear interpolation between mole fractions at designated baseline nodes, the latter being optimised as part of the state vector in the inversion. However, there were times when the simulated smooth baseline was not able to follow apparent fast changes in the observed baseline signal. For example, this was the case when the general advection direction towards Switzerland quickly changed from west to east, with mole fractions often being considerably elevated during easterly advection. At such transition times using the smooth baseline may lead to attribution errors in the emission field. Instead of a smooth baseline it would have been desirable to take the baseline directly from an unbiased state of a global scale model, sampling the mole fractions at the initial FLEXPART particle positions. However, such model output was not available for the investigation period at the time of the analysis.

Alternatively and to analyse the sensitivity of our set-up to these limitations, two additional baseline treatments were tested. The first (S-B1) was based on two baseline

Swiss methane emissions

S. Henne et al.

Title Page

Abstract

Introduction

Conclusions

References

Tables

Figures



Back

Close

Full Screen / Esc

Printer-friendly Version

Interactive Discussion



Swiss methane emissions

S. Henne et al.

Title Page

Abstract

Introduction

Conclusions

References

Tables

Figures



Back

Close

Full Screen / Esc

Printer-friendly Version

Interactive Discussion



estimations – one for the eastern and one for the western part of the inversion domain – which were combined using a weighted mean depending on the initial location of the model particles (here 4 days before arrival at the site). Since the initial location of the particles were available for every 3 h interval, this approach allows for more flexible variations of the simulated baseline signal. As in the standard baseline treatment, prior baseline mole fractions were taken from the REBS baseline at JFJ, applied here to both the eastern and western baselines. The second alternative baseline method (S-B2) extended the approach to a three-dimensional grid of baseline mole fractions accounting not only for east–west but also for north–south and vertical gradients. Again, the initial positions of the model particles within the grid as obtained from each FLEXPART simulation were used to determine the baseline concentration at the site as a weighted average. Different from methods B and S-B1, however, only one common set of gridded baseline mole fractions was estimated and applied to all sites. Only a very coarse ($3 \times 3 \times 2$) grid, covering the inversion domain, with a 15-daily temporal resolution was used in order to limit the size of the state vector. In the vertical, the grid was separating between heights 3000 m below and above ground level. The latter was chosen to assure that average initial sensitivities were similar for both vertical layers. Prior baseline values in the upper vertical layer were again taken from the REBS baseline at JFJ, whereas the lower layer was initialised with the REBS baseline at BEO. This assures a negative vertical gradient in CH_4 baseline mole fractions, since estimates for BEO were generally larger than those for JFJ.

3 Results

In the following the results of the emission inversions are presented, first in a more detailed fashion for the base inversion and second in a less exhaustive way for the sensitivity inversions highlighting the differences from the base case. Note that the base inversion does not necessarily represent the most likely or best estimate of the

posterior emissions. Rather, it is used as a starting point to analyse the sensitivity to different inversion settings.

3.1 Base inversion

Average source sensitivities as calculated with FLEXPART-COSMO on the reduced grid are shown in Fig. 1 for the base inversion as the combined sensitivity of the four sites BEO, LAE, SSL, and JFJ. Source sensitivities were largest close to the sites and in general for the Swiss Plateau (see Oney et al. (2015) for a detailed discussion of source sensitivities of the CarboCount-CH sites). The pronounced south-west to north-east orientation of the maximal source sensitivities is a result of the flow channeling between the Alps and the Jura mountains (Furger, 1990). South of the Alps and outside Switzerland source sensitivities quickly declined with generally larger values for westerly compared with easterly directions. Source sensitivities towards the south-east were especially small, reflecting the shielding effect of the Alps.

In Switzerland prior emissions amounted to 178 Ggyr^{-1} . After mapping the high resolution emission data to the reduced inversion grid (Fig. 2a) and applying Eq. (7), Swiss prior emissions were quantified at 183 Ggyr^{-1} . The difference of 2 % can be explained by mapping artefacts along the Swiss border. The distribution of the prior emissions (Fig. 2a) in Switzerland clearly emphasises the dominating role of emissions from the agricultural sector. Emission maxima are located in the Canton of Lucerne in close vicinity to BEO and in the north-eastern part of the country towards Lake Constance in the Cantons of Thurgau and Saint Gallen. All these areas are characterised by intensive agriculture with a focus on cattle farming. Emissions from the urban centres of Zurich, Basel, Bern and Geneva, in contrast, are not especially pronounced in the MAIOLICA inventory. Within the high Alpine area, and to a smaller degree within the Jura mountains, MAIOLICA emissions are significantly smaller, but are large again in the north Italian Po Valley and also in south-western Germany.

Simulated CH_4 time series for the sites used in the base inversion with low model release heights (B low) are compared with the observations in Fig. 3. Most of the time

Swiss methane emissions

S. Henne et al.

Title Page

Abstract

Introduction

Conclusions

References

Tables

Figures



Back

Close

Full Screen / Esc

Printer-friendly Version

Interactive Discussion



Swiss methane emissions

S. Henne et al.

Title Page

Abstract

Introduction

Conclusions

References

Tables

Figures



Back

Close

Full Screen / Esc

Printer-friendly Version

Interactive Discussion



the prior simulations were closely following the observed variability, underlining the very good performance of the transport model. However, during some periods the prior simulations considerably underestimated the observed mole fractions. This was especially true for the BEO and LAE sites and a period in March/April 2013. Some of the observed temporal variability was common for all sites suggesting an important influence from large-scale weather systems, whereas at other times the signals from different sites were little correlated. The two sites on the Swiss Plateau showed the most common behaviour, while, as expected, the high altitude observations at JFJ were most decoupled from the other observations. Also as expected, peak mole fractions were larger for the sites closer to the emissions (BEO, LAE) and smaller for the higher altitude sites (SSL and especially JFJ). The transport model captured this general tendency very well. Except for JFJ prior baseline mole fractions were smaller than most observed mole fractions.

The model's skill considerably improved for the posterior simulations showing greater correlations and lower biases. The simulations more closely followed the observed variability and the bias was reduced (Fig. 3). Partly, this was achieved through changes in the baseline mole fractions. Posterior baselines were generally greater than the prior at the BEO, LAE and SSL sites, whereas they were lower than the prior at JFJ. Largest baseline increases occurred during extended periods of elevated CH₄ (e.g. March 2013). These periods were characterised by easterly advection on the south-easterly side of high pressure systems with centres over north-western to central Europe. In these situations the limited model domain and the relatively short backward integration time of four days were likely insufficient to capture all recent emission accumulation above the baseline as observed at JFJ. As a consequence, the inversion adjusted the baseline upward.

The quality of the simulated time series is summarised in Fig. 4 where coefficients of determination, R^2 , are given for all sites, for both prior and posterior simulations and separately for the complete (Fig. 4a) and above-baseline signal (Fig. 4b). The performance in the prior simulations ranged from $R^2 = 0.25$ for the site FRU to $R^2 = 0.5$

for the site GIM and the complete signal. The coefficients of determination for the above baseline signal were slightly lower, but showed the same ranking between the sites: largest at GIM followed by the sites SSL, LAE, BEO and JFJ and smallest for FRU. Posterior coefficients of determination considerably increased for all sites used in the inversion ($R^2 = 0.58\text{--}0.69$), slightly increased for FRU, but slightly decreased for GIM. Improvements were seen both for the complete signal as well as for the above-baseline signal. The ranking between the sites remained similar after the inversion.

An overall quality indicator, which not only accounts for the correlation but also for a correct representation of the amplitude of the variability, is the Taylor skill score (Taylor, 2001)

$$S = \frac{4(1 + R)}{(\sigma_f + \sigma_f^{-1})^2 (1 + R_0)}, \quad (13)$$

where R is the Pearson correlation coefficient, R_0 the maximal attainable Pearson correlation of a “perfect” simulation, which is still limited by factors such as observation and representativeness uncertainty and was set to 0.9. $\sigma_f = \sigma_m / \sigma_o$ is the simulated standard deviation normalised by the observed standard deviation. S takes the value of 1 for a perfect simulation, but would take a value of 0.65 for perfectly correlated simulations that under/overestimate the observed variability by a factor of 2. The prior value of σ_f was well below 1 for all sites (0.43 to 0.71), indicating generally under-predicted peak heights, but increased in the posterior simulation to values between 0.65 to 0.8, except for GIM where it remained at 0.44. Posterior values of S for all sensitivity inversions and all sites are given in Table 4. For the base inversion S ranged from 0.78 to 0.91 for the sites used in the inversion and was smaller for the sites FRU and GIM (0.77 and 0.50). Note however, that for the latter two sites the baseline was not adjusted by the inversion, which may explain part of the weaker posterior performance. In the case of GIM it is remarkable that the correlation was comparatively large but the normalised standard deviation was very small. This may indicate that the general flow to the site

Swiss methane emissions

S. Henne et al.

Title Page

Abstract

Introduction

Conclusions

References

Tables

Figures



Back

Close

Full Screen / Esc

Printer-friendly Version

Interactive Discussion



was well captured by the transport model, but that either local boundary layer heights or local emissions were overestimated or underestimated, respectively. Taylor skill scores were very similar for posterior simulations of the base inversion using the high particle releases (B high in Table 4). Also, the prior simulation's performance was similar for low and high release heights, with lower release heights usually performing slightly better in terms of amplitude of the simulated variability and higher release heights showing slightly improved correlations. No clear preference for the lower or higher release height could be deduced from these results.

As an additional validation parameter the root mean square error (RMSE) and its reduction from prior to posterior simulations are shown in Fig. 4c and d. For sites used in the inversion the prior RMSE was between 20 and 40 nmol mol⁻¹ and decreased by 15 to 25% in the posterior simulations. For the near-surface sites FRU and GIM the RMSE did not significantly decrease after the inversion. At both sites simulated mole fractions were smaller than observed, especially at GIM. Even when using only afternoon values and when filtering for wind conditions with possibly large local influences (as done here), the transport model was not able to reproduce the amplitude of the observed variability at these sites. A reason for this poor model performance in FRU is most likely the inlet height very close to the surface and the associated high sensitivity to local emissions that cannot be captured at the resolution of the transport model. In GIM local emissions or mismatches in the local boundary layer height seem to be the main problem since the timing of the temporal variability was captured very well. The effect of including the sites GIM and FRU in the inversion is further discussed in Sect. 3.7.

Our model performance parameters are well within the range reported by other regional scale inversion studies of CH₄ surface fluxes for the European and East Asian domain using continuous observations and applying similar transport models as in our study (Bergamaschi et al., 2015; Manning et al., 2011; Thompson et al., 2015).

The posterior CH₄ emissions and their differences from the prior emissions are shown in Fig. 2b–d. The largest, though still modest, absolute changes (Fig. 2c) were

Swiss methane emissions

S. Henne et al.

Title Page

Abstract

Introduction

Conclusions

References

Tables

Figures



Back

Close

Full Screen / Esc

Printer-friendly Version

Interactive Discussion



5 estimated for the region south-west of BEO. In this region with large prior emissions from agriculture, reductions were in the order of 25 %. Further reductions were estimated east of the site LAE in the canton of Thurgau (please refer to Fig. S1 for a map of the Swiss cantons) and in large parts of western Switzerland. In contrast, larger than
10 prior emissions were obtained for north-eastern Switzerland in the Cantons of Saint Gallen and Appenzell and also beyond the border in south-western Bavaria. Emissions in northern Italy were increased but due to the weak sensitivity for this region these posterior results are subject to larger uncertainties than those on the Swiss Plateau. Relative emission increases (Fig. 2d) of up to 30 % were detected for the Appenzell region and the bordering Vorarlberg region in Austria. On the contrary, relative emission reductions appeared for the southern Black Forest. Similar patterns emerged for the base inversion when using the high release heights (see Fig. S3 in the Supplement), but posterior emissions were generally larger in this case.

15 In this base inversion Swiss total emissions were estimated at $179 \pm 7 \text{ Ggyr}^{-1}$ (1σ) and $195.0 \pm 7.3 \text{ Ggyr}^{-1}$ for the low and high particle release heights, respectively. Both values are not significantly (two-sided Welch t test) different from their prior value, indicating a high level of consistency between the bottom-up estimate of the MAIOLICA inventory and our top-down estimate. Furthermore, analytical uncertainties of the posterior were considerably reduced by about 75 %. However, an additional uncertainty range of $\pm 15 \text{ Ggyr}^{-1}$ is introduced by the choice of the particle release height.

20 Next to an improved reproduction of the measurement time series, the reduction of uncertainty in the emission field provides information on the quality of the inversion. Uncertainty reductions were largest close to the observation sites (Fig. 5). For the sites with larger surface sensitivities (LAE and BEO), uncertainty reductions in their vicinity were larger than for the more remote sites (SSL and JFJ). It is interesting to note that uncertainty reductions were largest in the area around and west of BEO, where also emission reductions were the largest. Uncertainty reductions were smaller for the area east of LAE, where also considerable emission reductions were established. For
25 north-eastern Switzerland, where the inversion produced large emission increases,

uncertainty reductions were relatively small. The associated emission increases are thus less well constrained, which in turn may indicate temporally variable emissions or increased transport uncertainties for the associated flow direction.

3.2 Seasonal cycle

When allowing seasonal variability of the emission fluxes (S-V), distinct differences between the seasons are visible, although no seasonal variability was included in the prior (Figs. 6 and S4 in the Supplement). Winter-time posterior emissions were strongly reduced especially in agricultural areas. Posterior emissions during the other seasons tended to be slightly larger than their prior values.

Also the estimated emission patterns changed from season to season. In spring and summer increased posterior emissions were estimated for eastern Switzerland, the Canton of Lucerne (around BEO) and generally the pre-alpine area, whereas there was a tendency for smaller than prior emissions in western Switzerland. The strong increase around the station FRU (not used in the inversion) is consistent with the observation that the posterior model performance for the site FRU was considerably enhanced compared to the prior simulation. Performance was also enhanced compared to the posterior simulation of the base inversion both in terms of correlation and RMSE reduction, although Taylor skill scores were similar in both inversions (see Table 4). On the contrary, during fall higher than prior emissions were present in north-western and eastern Switzerland, and for small areas south of BEO and east of LAE posterior emissions were below prior estimates.

For the low model release height, total Swiss emission rates were smallest during winter ($152.2 \pm 9.7 \text{ Ggyr}^{-1}$) but were relatively similar and close to the prior estimates during the other seasons (206.5 ± 12 , 182.1 ± 13 , and $202.7 \pm 11 \text{ Ggyr}^{-1}$ for spring, summer and autumn, respectively). The annual total Swiss emissions for S-V were $185.9 \pm 6.5 \text{ Ggyr}^{-1}$, very close to those of the base inversion. Winter-time emission rates were 18% smaller than the annual mean. For the high model release heights, a similar but less pronounced annual cycle was derived, which featured total annual

Swiss methane emissions

S. Henne et al.

Title Page

Abstract

Introduction

Conclusions

References

Tables

Figures



Back

Close

Full Screen / Esc

Printer-friendly Version

Interactive Discussion



emissions of $197 \pm 7 \text{ Ggyr}^{-1}$ and winter-time emission rates of $171 \pm 10 \text{ Ggyr}^{-1}$ (13 % lower than annual mean).

3.3 Extended Kalman Filter inversion

The extended Kalman filter inversion using low particle release heights (S-K low) yielded similar annual mean posterior emissions as the base inversion (Figs. 7 and S5 in the Supplement). Several features of the posterior emission differences obtained by the base inversion are also visible in the extKF inversion: reductions west of BEO, increases in north-eastern Switzerland, small changes in the Alpine area, small increase in the region close to GIM (shifted south-westerly as compared to base inversion). No emission reductions were, however, deduced for the area east of LAE. Overall the posterior model performance using the extKF inversion was superior (S between 0.84 and 0.95) compared to the base inversion (Table 4), which may be related to the time variable posterior emission field and/or the different treatment of baseline mole fractions.

Total Swiss emissions were estimated at 193 ± 13 and $217 \pm 14 \text{ Ggyr}^{-1}$ by the extKF inversion for the low and high particle release height, respectively. These values are considerably larger (8 and 15 %) than those of the base inversion but fall well within the range of values reported by the other sensitivity inversions using the Bayesian approach. The difference in total emissions between the low and high release case of 24 Ggyr^{-1} was considerably larger than in the base inversion (Table 4). Uncertainty estimates of the posterior emissions remained larger in the extKF case than in the base inversion, despite the fact that similar prior uncertainties and model/observation uncertainties were used in both systems. The main reason for this observation is that the uncertainties of the state vector are allowed to grow in the extKF from one time step to the next accounting for the forecast uncertainty, which introduces an additional amount of prior uncertainty.

Swiss methane emissions

S. Henne et al.

Title Page

Abstract

Introduction

Conclusions

References

Tables

Figures



Back

Close

Full Screen / Esc

Printer-friendly Version

Interactive Discussion



3.4 Influence of transport model

In the sensitivity case S-EC the source sensitivities were derived from FLEXPART-ECMWF instead of FLEXPART-COSMO (see Sect. 2.2). On the one hand, FLEXPART-ECMWF may be less suitable to resolve the complex flow in the Swiss domain due to its coarser horizontal resolution. On the other hand, FLEXPART-ECMWF is a well validated model code and has been widely used for inverse modelling (e.g. Stohl et al., 2009; Thompson and Stohl, 2014; Thompson et al., 2015). Using the same inversion settings, FLEXPART-ECMWF simulations yielded generally similar posterior emissions as the base inversion (Figs. 8 and S6 in the Supplement). Common features were again the decrease west of BEO and east of LAE and the increase in north-eastern Switzerland with respect to the prior emissions. In contrast to the base inversion, large emission reductions were also assigned to most of the western part of the country towards lake Geneva. For the low release height, the model performance at the observation sites was only slightly lower compared to the base inversion as indicated by the posterior Taylor skill scores (Table 4). In contrast, posterior Taylor skill scores were slightly larger in the high release case than in the base inversion. An exception was the GIM site, for which skill scores were strongly reduced using FLEXPART-ECMWF. This may reflect the growing inability of a coarser transport model to simulate the local CH₄ contribution to the site.

Although FLEXPART-ECMWF's performance at the sites was of similar quality as for the base inversion, the uncertainty reductions of the posterior emissions (Fig. 8b) were not as pronounced in the S-EC cases (low and high) as compared to the base inversion. Again, this is a hint that the coarser model's transport simulations are not as accurate and therefore lead to a less clear identification of the emission sources. Total Swiss posterior emissions in the S-EC case were 171.1 ± 8.0 and 182.1 ± 7.6 Ggyr⁻¹ in the low and high particle release case, respectively, slightly smaller than in the base inversion. One possible explanation may be the coarser and, hence, potentially less dispersive behaviour of FLEXPART-ECMWF. Mesoscale flow patterns in complex ter-

Swiss methane emissions

S. Henne et al.

Title Page

Abstract

Introduction

Conclusions

References

Tables

Figures



Back

Close

Full Screen / Esc

Printer-friendly Version

Interactive Discussion



in the S-E case were also large for the urban areas (Fig. 9b), lending credibility to the associated emission reductions.

3.6 Influence of covariance treatment

The inversion results using the model/observation uncertainty as estimated by the method of Stohl et al. (2009) (S-S) were smaller than in the base inversion in the low release case but differed only slightly in the high release case (see Table 4). In S-S an almost constant uncertainty (see Sect. 2.4) was given to all model/observation pairs of one site, while in the base inversion uncertainties tended to be larger for large above-baseline mole fractions. However, model uncertainties were mostly smaller for the base inversion except for 10 to 20 % of the observations in the “low” and less than 10 % in the “high” release case. Despite these differences in the applied model uncertainty, the distribution of posterior fluxes was similar to that of the base inversion with two exceptions: emission reductions were more pronounced in the area west of BEO and east of LAE in the S-S case and additional reduction occurred around the BEO site itself (see Fig. S9 in the Supplement). The distinct posterior increase in north-eastern Switzerland was also present in S-S.

In comparison with the base inversion, all parameters describing the uncertainty covariance matrices showed increased values when they were estimated by the maximum likelihood method (Table 3). Especially the uncertainty of the baseline, as described by parameter f_b , was strongly increased for all sites, but also the model uncertainties were generally larger (parameters σ_{\min} and σ_{srr}). In addition, the ML method yielded an increased uncertainty of the prior emissions, resulting in a total uncertainty for Switzerland of about 30 %, indicating that the bottom-up estimate of 16 % may be too optimistic. The spatial correlation length of the prior emissions remained very close to the $L = 50$ km used in the base inversion. The resulting posteriori emissions were distributed similarly as in the base inversion. However, emission reductions were more pronounced (see Fig. S10 in the Supplement). As for the S-S sensitivity, emission reductions were also estimated for the region between BEO and LAE and only a small

Swiss methane emissions

S. Henne et al.

Title Page

Abstract

Introduction

Conclusions

References

Tables

Figures



Back

Close

Full Screen / Esc

Printer-friendly Version

Interactive Discussion



Swiss methane emissions

S. Henne et al.

Title Page

Abstract

Introduction

Conclusions

References

Tables

Figures



Back

Close

Full Screen / Esc

Printer-friendly Version

Interactive Discussion



local increase around the BEO site remained. The total posterior emissions for Switzerland were only 158 ± 13 and 169 ± 13 Ggyr⁻¹ for the low and high particle release case, respectively. Due to the larger baseline uncertainty as estimated by the ML optimisation, adjustments of the posterior baseline were larger than in the base inversion. As a result baseline mole fractions were raised for the sites BEO and LAE during periods of increased CH₄ observations, hence, reducing the need for increased emissions at these times and lowering the overall posterior emissions. The increased prior and model uncertainties resulted in relatively large posterior uncertainties as compared with the base inversion. The overall posterior model performance was similar to that of the base inversion. However, a larger part of the the simulated variability was attributed to variations in baseline signal.

3.7 Influence of observation selection

For almost all sensitivity inversions with different subsets of observational data (S-O1 to S-O5 in Table 2) the emission reduction west of BEO could be confirmed (see Figs. S11, S12, S13, S14, S15 in the Supplement). In contrast, the reduction east of LAE was only evident in those runs that also used the observations from LAE. Similarly, the increase in north-eastern Switzerland was more pronounced if the observations from BEO were used. Relatively large emission changes were obtained at mid range (100 to 500 km) from the sites on the Swiss Plateau when the more remote sites SSL and JFJ were not used in the inversion (S-O1 to S-O3). The larger emission changes in S-O1 to S-O3 were likely the result of shadowing effects: the BEO and LAE sites were only sensitive to these distant areas when they were also sensitive to closer emission sources resulting in a false attribution of emissions to distant areas located behind the real emission sources. Using observations from additional sites with a different sensitivity pattern can solve this problem as it did in our base inversion.

Swiss CH₄ emissions for this set of sensitivity inversions were larger than in the base inversion (Table 4). Largest emissions (214.3 ± 11 Ggyr⁻¹ in the low release case) were obtained when only the site LAE was used (S-O2), resulting in large emission

increases in western Switzerland, whereas posterior emissions remained similar to the base inversion close to the BEO and LAE sites. This pattern is most likely due to the problem of shadowing effects.

S-O5, the inversion using all six sites, resulted in comparatively large total emissions for Switzerland as well ($208.8 \pm 6 \text{ Ggyr}^{-1}$ in the low release case). Emissions were largely increased around the site GIM and further west as a result of the large mole fractions observed at GIM. As discussed earlier, it seems likely that large local emissions around GIM could not properly be accounted for by the inversion system and were spread out over a larger area, resulting in overall larger national emissions.

It is interesting to note that including the additional observations only slightly reduced the overall uncertainty of the national emission estimate in comparison to the base inversion (from 7.0 to 6.0 Ggyr^{-1} for the low release case). In contrast, using the two sites LAE and BEO in combination instead of either one of them individually, reduced the uncertainty from about 11 to 7.9 Ggyr^{-1} . Hence, the additional gain in terms of uncertainty reduction was relatively small when adding the sites GIM and FRU, which is another indication of their more localised sensitivity and, hence, reduced value in the inversion.

Of the sensitivity inversions with differing observation data the results of the case using only observations from BEO (S-O1) was closest to those of the base inversion, both in terms of total emissions and of geographic distribution. This supports the expectation that a tall tower site should be best suited for inverse modelling and may allow the estimation of other Swiss GHG fluxes using observations from this site alone.

3.8 Influence of baseline treatment

Comparing the inversion results of the two inversions with alternative baseline treatment (S-B1 and S-B2; see Sect. 2.5 for details) with the base inversion did not reveal any large differences in terms of geographical distribution (see Figs. S16 and S17 in the Supplement). Especially S-B2 yielded enhanced model performance that was mainly due to a more detailed description of the temporal variability of the baseline (Table 4).

Swiss methane emissions

S. Henne et al.

Title Page

Abstract

Introduction

Conclusions

References

Tables

Figures



Back

Close

Full Screen / Esc

Printer-friendly Version

Interactive Discussion



Swiss methane emissions

S. Henne et al.

Title Page

Abstract

Introduction

Conclusions

References

Tables

Figures



Back

Close

Full Screen / Esc

Printer-friendly Version

Interactive Discussion



Total Swiss emissions for S-B1 remained very similar to the base inversion but were considerably larger for S-B2 (195.1 ± 6.9 and 223.6 ± 6.9 Ggyr⁻¹ for low and high particle release height, respectively). In S-B2, where a coarse three-dimensional grid of baseline mole fractions was optimised, their posterior values were largest for the eastern and low grid cells and during the previously highlighted period in March 2013 and again in the winter 2013/14. Furthermore, vertical gradients were smaller during the summer months than during the winter (see Fig. S18 in the Supplement). This general distribution is in line with our expectations (higher mole fractions towards surface and more continental areas) and lends credibility to this kind of baseline estimation. One further advantage of analysing a common baseline grid for all sites is its possible use for the validation sites as well. Indeed, a larger improvement in posterior performance at the sites FRU and GIM can be seen for S-B2 than in any other sensitivity inversion in which the sites were used for validation only.

4 Discussion

4.1 National total emissions

The main result of the present study is summarised in Fig. 10 in terms of a histogram of total Swiss CH₄ emissions for the investigation period March 2013 to February 2014 taken from all sensitivity inversions. The estimates from the individual sensitivity inversions almost follow a normal distribution. A clear average difference between sensitivity runs using the high and low particle release heights of 20 Ggyr⁻¹ is apparent. This difference is larger than the one between the results taken from the two employed transport models FLEXPART-ECMWF and FLEXPART-COSMO (12 Ggyr⁻¹, 5 %). The latter supports the large degree of consistency between the two transport models and the underlying meteorology. In an inverse estimate of HFC-134a emissions from the continental USA, Hu et al. (2015) had observed a somewhat larger emission difference

Swiss methane emissions

S. Henne et al.

Title Page

Abstract

Introduction

Conclusions

References

Tables

Figures



Back

Close

Full Screen / Esc

Printer-friendly Version

Interactive Discussion



posterior uncertainty of individual inversions may be seen in the small prior uncertainty of 16 % for the national total. Similarly, when applying the the ML method, considerably larger prior uncertainties in the range of 30 % were suggested (see Sect. 3.6). However, posterior uncertainties of the ML sensitivity runs (S-ML in Table 4) were still considerably smaller than our overall uncertainty. Another reason for small posterior uncertainties could be an underestimated model/observation uncertainty, lending too much trust to the simulation of the observations and in turn reducing posterior uncertainties. However, model/observation uncertainties were optimised in the same step as prior uncertainties with the ML method and were not estimated to be considerably different from the base setup (see Table 3). These considerations lead to the conclusion that the enhanced posterior uncertainty over all sensitivity runs needs to be seen as the contribution of systematic uncertainties that are introduced by the specific setup of the inversion system and cannot be fully covered by the analytical estimate of the Bayesian analysis, a result that has also been obtained in previous inversion studies (e.g. Bergamaschi et al., 2010, 2015).

4.2 Spatio-temporal emission patterns

Considerable emission differences were observed between the seasons, with winter-time emissions being 13 to 18 % lower than the annual average. Since the largest winter-time reduction was deduced for areas with large cattle density, it seems very likely that the estimated reductions are connected with the agricultural sector. When referred to the prior emissions from the agricultural sector only (150 Ggyr^{-1} , FOEN, 2014), the estimated seasonal posterior variability would be around 22 %. The latter is well in line with Gao et al. (2011) who estimated the seasonal variability of CH_4 emissions from a dairy cow farmstead in northern China. A major contribution to the annual variability may stem from CH_4 emissions from manure handling and storage, which strongly depends on temperature. Zeitz et al. (2012) speculated that Swiss CH_4 emissions from manure handling should be lower than estimated by FOEN (2014), since their observed emission factors were significantly smaller than those suggested

Swiss methane emissions

S. Henne et al.

Title Page

Abstract

Introduction

Conclusions

References

Tables

Figures



Back

Close

Full Screen / Esc

Printer-friendly Version

Interactive Discussion



by IPCC and used by FOEN (2014). However, their results were based on laboratory experiments that yet need to be validated in the field. Furthermore, Zeitz et al. (2012) suggest that emissions from manure handling should be significantly reduced or even cease during winter, considering the average temperatures in Switzerland. Accounting for the temperature of the manure storage, which may be well above the ambient temperature, in the emission calculation, a 50 % wintertime reduction was estimated in the bottom-up inventory (FOEN, 2015). Furthermore, seasonal variability in emissions from ruminants may be induced by seasonal variability of productivity, especially of dairy cows. In Switzerland it is common practice to time the calving date in the spring so that the cows reach their largest productivity at the point of largest feed availability (spring/summer). Since productivity and CH₄ emissions are roughly proportional, direct ruminant emissions should also follow a seasonal cycle with a minimum in the winter months (FOEN, 2015). The temporal variability in our inversion results largely agrees with these considerations and, hence, fits well to our understanding of the main agricultural emission processes in Switzerland. Furthermore, we had seen that mean annual posterior emissions were about 10 to 20 % lower in agricultural areas in our base inversion (B low). Taking the mean over all sensitivity inversions this reduction is around 5 to 15 % as compared to the prior, which was based on the 2014 reporting. Considering the larger emissions from agriculture in the 2015 reporting, our mean posterior emissions in agricultural areas suggest that the revised bottom-up inventory (FOEN, 2015) overestimates agricultural emissions by 10 to 20 %. From the inferred seasonality we conclude that this is most likely because emissions from manure handling are overestimated. Our findings are in contrast to recent, somewhat controversial studies in the USA that find a significant underestimation of ruminant emissions in the EDGAR-v4.2 and USA EPA inventories (Miller et al., 2013; Wecht et al., 2014; Turner et al., 2015).

Our posterior results depend little on the prior emission distribution (B vs. S-E and S-T) and corrected the large emissions in urban areas given by the EDGARv4.2 inventory downwards. Hence, we conclude that the emissions from natural gas distribution and use in the SGHGI/MAIOLICA inventory is more realistic than in EDGARv4.2. The

Swiss methane emissions

S. Henne et al.

Title Page

Abstract

Introduction

Conclusions

References

Tables

Figures



Back

Close

Full Screen / Esc

Printer-friendly Version

Interactive Discussion



SGHGI emissions from natural gas distribution of 8 Ggyr^{-1} correspond to $< 0.4\%$ of the Swiss natural gas consumption (FOEN, 2015). This is in contrast to recent studies from the USA where a large underestimation of fugitive emissions was established in the inventories for different metropolitan areas (Wennberg et al., 2012; McKain et al., 2015) and fractional loss rates between 2.5 and 6% were established. According to the SGHGI, fugitive emissions were reduced in Switzerland by 36% since 1990 mainly due to a gradual replacement of cast-iron pipes by polyethylene pipes (FOEN, 2015). Our results support the reductions documented in the SGHGI and, thus, the success of this emission reduction measure. This also highlights that large reduction potentials can be expected for other countries as well when modernisation of the infrastructure is promoted.

CH_4 emissions from composting and anaerobic digestion (IPCC 5B), mainly in the conversion of biogenic waste to biogas in small scale facilities, were amended from 5 to 16 Ggyr^{-1} from the 2014 to the 2015 reporting (Table 5). In our prior inventory, these emissions were not explicitly localised (Hiller et al., 2014a). Since our prior was based on the earlier 5 Ggyr^{-1} estimate, an increase in regions with intensive biogas production should have been detectable. However, the biogas and composting plants are approximately evenly distributed across the Swiss Plateau in areas of dominating agricultural use. Hence, it is impossible to finally attribute any of the observed posterior emission differences to this emission process. Similarly and as already indicated by Hiller et al. (2014a), emissions from waste water treatment were probably underestimated in previous FOEN estimates. In the most recent reporting from 2015, these emissions were 6.77 Ggyr^{-1} , which is an increase by a factor of 15 compared to previous reports. The spatial distribution of CH_4 emissions from waste water treatments should mainly follow the population density. Although, our inversion results do not support increased emissions in densely populated areas, the relatively small emission revision (compared to the total emissions) may be very difficult to detect.

4.3 Unidentified source in north-eastern Switzerland

The largest emission changes that were localised by the inversion and were present in almost all sensitivity inversions were those in the north-eastern part of Switzerland in the Cantons of Saint Gallen and Appenzell. These areas are also dominated by agriculture and the estimated increase, hence, contradicts the reductions in other agricultural regions. One possible reason for the increase could be systematic biases in the transport simulations. One argument against this possibility is that the increase was observed also when using FLEXPART-ECMWF instead of FLEXPART-COSMO (see Sect. 3.4) and it seems unlikely that the same systematic bias would be inherent to both meteorological inputs. Another possible reason for the increased emissions could be an emission source close to the observational sites that could not be described correctly by the limited model resolution and whose contributions were wrongly assigned to the respective area. Again, this seems unlikely, since the increase was present in sensitivity inversions using either one of the sites on the Swiss Plateau (S-O1, S-O2). In conclusion, it seems likely that the estimated increase represents a real emission source that is not present or under-estimated in our prior inventory.

This raises the question which processes may be responsible for the detected emissions. A possible candidate is an erroneous spatial distribution of ruminant emissions within Switzerland. However, in Switzerland the number of ruminants by animal species needs to be reported at the farm level and this information, aggregated to communities, was used for distributing agricultural emissions in the prior inventory (Hiller et al., 2014a). Different cow breeds may have different CH₄ emissions factors. The dominating breeds in Switzerland are Brown Swiss and Holstein, for which similar emissions factors have been reported (Felber et al., 2015, and references therein). Different management methods and diet types may also lead to slight variations in the emission factors. To our knowledge, detailed investigations of emission factors under real Swiss farming conditions are currently not available. Therefore, effects of herd composition and management cannot be excluded, although it seems unlikely that these could fully

Title Page

Abstract

Introduction

Conclusions

References

Tables

Figures



Back

Close

Full Screen / Esc

Printer-friendly Version

Interactive Discussion



Swiss methane emissions

S. Henne et al.

Title Page

Abstract

Introduction

Conclusions

References

Tables

Figures



Back

Close

Full Screen / Esc

Printer-friendly Version

Interactive Discussion



explain the differences estimated by the inversion. A typical farming practice in Switzerland is moving grassing cows towards elevated Alpine pastures during the summer months. This was considered in the prior by redistributing 4 % of the national ruminant emissions to Alpine pastures (Hiller et al., 2014a). Although there are extended areas of Alpine pastures present in north-eastern Switzerland, these are not more prominent than in other Alpine areas where we did not observe increased posterior emissions. Furthermore, increased emissions in north-eastern Switzerland were also observed by the inversion for the winter and spring periods, when the Alpine pastures are unoccupied. Possible additional sources of anthropogenic CH₄ in north-eastern Switzerland may stem from biological treatment of waste in composting and anaerobic digestion facilities, solid waste disposal, waste water treatment, and natural gas distribution. Currently we have no indication that either of these processes shows a specifically high density in the given area.

This leaves the possibility of an underestimated or unaccounted natural CH₄ source. The net natural emissions accounted for by Hiller et al. (2014a) were very small ($\approx 3 \text{ Ggyr}^{-1}$) compared to their anthropogenic counterpart ($\approx 180 \text{ Ggyr}^{-1}$). Emissions from wetlands and lakes are thought to be the largest natural source in Switzerland (4.6 Ggyr^{-1}). Although there are a number of small wetlands and lakes situated in the Cantons of Appenzell, their fractional coverage and total area is not larger than in other areas (for example Entlebuch south-west of BEO). Furthermore, we have no indication that climate variability within the domain could have impacted the drivers of wetland emissions (precipitation, temperature) in an inhomogeneous way to explain large regional differences. Aerobic soils (forest and agricultural) are generally thought to be CH₄ sinks and were estimated to contribute a negative CH₄ flux of -4.3 to -2.8 Ggyr^{-1} (Hiller et al., 2014a). Nevertheless, under anaerobic conditions methanogenesis may dominate in deep organic soils, which can be found in wetland or peatland areas. When former peatlands are re-wetted (either due to accidental flooding or renaturation) they have been shown to become a significant CH₄ source depending on water table depth, the abundance of vascular vegetation transporting CH₄ from the root space to the at-

Swiss methane emissions

S. Henne et al.

Title Page

Abstract

Introduction

Conclusions

References

Tables

Figures

◀

▶

◀

▶

Back

Close

Full Screen / Esc

Printer-friendly Version

Interactive Discussion



mosphere and the amount of available carbon in plant litter (Couwenberg and Hooijer, 2013). Organic soils were not considered as CH₄ sources in our prior. One large area of deep organic soils in Switzerland is located in the Alpine Rhine valley (Wüst-Galley et al., 2015), only slightly east of the area of our largest posterior increase. This possible source though remains uncertain since the area in question is used for agriculture and should be well drained throughout most of the year. The only other large area of converted peatland in Switzerland is the Seeland region around the GIM site, possibly contributing to the large CH₄ concentrations observed there (see Sects. 2.1 and 3.1). Admittedly, river re-routing and drainage systems should keep the water table low in this area. In conclusion, we cannot explicitly determine which process may have caused the increased posterior emissions in north-eastern Switzerland. Additional studies using data from more recent observations and/or additional sites will be needed to clarify these open questions.

5 Conclusions

We applied a high resolution atmospheric transport model to simulate the CH₄ observations of the CarboCount-CH network and used inversion techniques to estimate total Swiss CH₄ emissions and their geographical distribution for the period March 2013 to February 2014. A series of sensitivity inversions (varying the treatment of temporal variability of the emissions, the transport model, the inversion algorithm, the prior emissions, the uncertainty covariance matrices, the selected observations, and the baseline treatment) confirm the robustness and independent character of our results.

Our best estimate of total Swiss CH₄ emissions ($196 \pm 18 \text{ Ggyr}^{-1}$) largely supports the bottom-up estimate as reported by the Swiss Federal Office for the Environment ($206 \pm 33 \text{ Ggyr}^{-1}$). The overall uncertainty as obtained from all sensitivity inversions (10 %) was larger than the analytical uncertainty of any individual sensitivity inversion, but still considerably reduced the uncertainty associated with the bottom-up estimate (16 %).

Swiss methane emissions

S. Henne et al.

Title Page

Abstract

Introduction

Conclusions

References

Tables

Figures



Back

Close

Full Screen / Esc

Printer-friendly Version

Interactive Discussion



The inversion results indicate a redistribution of CH₄ as compared to the spatially explicit bottom-up inventory. Large winter time posterior emission reductions in regions dominated by agricultural emissions suggest that these are overestimated on an annual basis by 10 to 20 % in the most recent bottom-up inventory and that manure handling may be the responsible process. Our findings are in contrast to recent studies from the USA that suggested considerably larger emissions from ruminants than reported in bottom-up inventories (Miller et al., 2013; Wecht et al., 2014; Turner et al., 2015). An area of increased posterior emissions in north-eastern Switzerland could not be assigned to a single most likely source process. Emissions from previously drained peatlands may be responsible for this observation. However, this suggestion needs further investigation.

Bottom-up estimates indicate that Swiss national emissions decreased by about 20 % since the 1990s, mainly due to a reduction in livestock numbers and improvements in the gas distribution network (FOEN, 2015). The latter can be supported by our study, which did not assign large emissions to densely populated areas and strongly corrected such emissions when present in the prior estimate (EDGAR inventory). This again is in contrast to recent studies from the USA that showed larger than expected emissions from natural gas distribution (Wennberg et al., 2012; McKain et al., 2015) and provides evidence for the efficiency of comparatively simple modernisation efforts to reach greenhouse gas reduction targets.

Our results also demonstrate the feasibility of using high-resolution transport models and continuous atmospheric observations to deduce regional scale surface fluxes with a horizontal resolution required to retrace the underlying emission/uptake processes. This conclusion is especially encouraging when considering the complex topography of the study area. Furthermore, it is a prerequisite for studying the more complex exchange of carbon dioxide between the terrestrial biosphere and the atmosphere. Inversion results using data from two sites on the Swiss Plateau and two elevated sites (base inversion) were consistent with a sensitivity inversion that used only the tall tower observations of Beromünster (212 m.a.g.l.). The latter emphasizes the special value of

tall tower observations in deriving regional scale fluxes. Sustaining a dense observational network like CarboCount-CH will allow for independent monitoring of future climate agreements.

**The Supplement related to this article is available online at
doi:10.5194/acpd-15-35417-2015-supplement.**

Acknowledgements. This study was funded by the Swiss Federal Office for the Environment (FOEN) and by the Swiss National Science Foundation (SNSF) as part of the “CarboCount CH” Sinergia Project (Grant Number: CRSII2_136273). We thank the International Foundation High Altitude Research Stations Jungfraujoch and Gornergrat (HFSJG) for the opportunity to perform experiments on the Jungfraujoch, MeteoSwiss for providing meteorological observations at the site Lägern Hochwacht and COSMO model analysis, and Swiss FLUXNET for the meteorological observations at Frübüel. Measurements at Jungfraujoch were partly performed as part of the Swiss contribution to ICOS (www.icos-infrastructure.eu).

References

- Baldauf, M., Seifert, A., Förstner, J., Majewski, D., Raschendorfer, M., and Reinhardt, T.: Operational Convective-Scale Numerical Weather Prediction with the COSMO Model: description and Sensitivities, *Mon. Weather Rev.*, 139, 3887–3905, doi:10.1175/MWR-D-10-05013.1, 2011. 35426
- Bamberger, I., Stieger, J., Buchmann, N., and Eugster, W.: Spatial variability of methane: attributing atmospheric concentrations to emissions, *Environ. Pollut.*, 190, 65–74, doi:10.1016/j.envpol.2014.03.028, 2014. 35420
- Bamberger, I., Oney, B., Brunner, D., Henne, S., Leuenberger, M., Buchmann, N., and Eugster, W.: Observation of atmospheric methane and carbon dioxide: tall tower or mountain top stations?, *Bound. Lay. Meteorol.*, in review, 2015. 35423
- Bergamaschi, P., Bräunlich, M., Marik, T., and Brenninkmeijer, C. A. M.: Measurements of the carbon and hydrogen isotopes of atmospheric methane at Izaña, Tenerife: sea-

Swiss methane emissions

S. Henne et al.

Title Page

Abstract

Introduction

Conclusions

References

Tables

Figures



Back

Close

Full Screen / Esc

Printer-friendly Version

Interactive Discussion



Swiss methane emissions

S. Henne et al.

Title Page

Abstract

Introduction

Conclusions

References

Tables

Figures



Back

Close

Full Screen / Esc

Printer-friendly Version

Interactive Discussion



sonal cycles and synoptic-scale variations, *J. Geophys. Res.-Atmos.*, 105, 14531–14546, doi:10.1029/1999JD901176, 2000. 35421

Bergamaschi, P., Krol, M., Dentener, F., Vermeulen, A., Meinhardt, F., Graul, R., Ramonet, M., Peters, W., and Dlugokencky, E. J.: Inverse modelling of national and European CH₄ emissions using the atmospheric zoom model TM5, *Atmos. Chem. Phys.*, 5, 2431–2460, doi:10.5194/acp-5-2431-2005, 2005. 35421

Bergamaschi, P., Krol, M., Meirink, J. F., Dentener, F., Segers, A., van Aardenne, J., Monni, S., Vermeulen, A. T., Schmidt, M., Ramonet, M., Yver, C., Meinhardt, F., Nisbet, E. G., Fisher, R. E., O'Doherty, S., and Dlugokencky, E. J.: Inverse modeling of European CH₄ emissions 2001–2006, *J. Geophys. Res.-Atmos.*, 115, D22309, doi:10.1029/2010JD014180, 2010. 35419, 35421, 35433, 35453

Bergamaschi, P., Houweling, S., Segers, A., Krol, M., Frankenberg, C., Scheepmaker, R. A., Dlugokencky, E., Wofsy, S. C., Kort, E. A., Sweeney, C., Schuck, T., Brenninkmeijer, C., Chen, H., Beck, V., and Gerbig, C.: Atmospheric CH₄ in the first decade of the 21st century: inverse modeling analysis using SCIAMACHY satellite retrievals and NOAA surface measurements, *J. Geophys. Res.-Atmos.*, 118, 7350–7369, doi:10.1002/jgrd.50480, 2013. 35421

Bergamaschi, P., Corazza, M., Karstens, U., Athanassiadou, M., Thompson, R. L., Pison, I., Manning, A. J., Bousquet, P., Segers, A., Vermeulen, A. T., Janssens-Maenhout, G., Schmidt, M., Ramonet, M., Meinhardt, F., Aalto, T., Haszpra, L., Moncrieff, J., Popa, M. E., Lowry, D., Steinbacher, M., Jordan, A., O'Doherty, S., Piacentino, S., and Dlugokencky, E.: Top-down estimates of European CH₄ and N₂O emissions based on four different inverse models, *Atmos. Chem. Phys.*, 15, 715–736, doi:10.5194/acp-15-715-2015, 2015. 35433, 35442, 35453

Berhanu, T. A., Satar, E., Schanda, R., Nyfeler, P., Moret, H., Brunner, D., Oney, B., and Leuenberger, M.: Measurements of greenhouse gases at Beromünster tall tower station in Switzerland, *Atmos. Meas. Tech. Discuss.*, 8, 10793–10822, doi:10.5194/amtd-8-10793-2015, 2015. 35423

Brunner, D., Henne, S., Keller, C. A., Reimann, S., Vollmer, M. K., O'Doherty, S., and Maione, M.: An extended Kalman-filter for regional scale inverse emission estimation, *Atmos. Chem. Phys.*, 12, 3455–3478, doi:10.5194/acp-12-3455-2012, 2012. 35432, 35434, 35435

Swiss methane emissions

S. Henne et al.

Title Page

Abstract

Introduction

Conclusions

References

Tables

Figures



Back

Close

Full Screen / Esc

Printer-friendly Version

Interactive Discussion



- Brunner, D., Henne, S., Keller, C. A., Vollmer, M. K., and Reimann, S.: Estimating European Halocarbon Emissions Using Lagrangian Backward Transport Modeling and in Situ Measurements at the Jungfrauoch High-Alpine Site, in: Lagrangian Modeling of the Atmosphere, edited by Lin, J. C., Gerbig, C., Brunner, D., Stohl, A., Luhar, A., and Webley, P., vol. 200 of Geophysical Monographs V, 207–221, AGU, Washington, DC, 2013. 35428
- Chen, Y. H. and Prinn, R. G.: Estimation of atmospheric methane emissions between 1996 and 2001 using a three-dimensional global chemical transport model, *J. Geophys. Res.-Atmos.*, 111, D10307, doi:10.1029/2005JD006058, 2006. 35421
- Couwenberg, J. and Hooijer, A.: Towards robust subsidence-based soil carbon emission factors for peat soils in south-east Asia, with special reference to oil palm plantations, *Mires and Peat*, 12, 1–13, 2013. 35458
- Dentener, F., van Weele, M., Krol, M., Houweling, S., and van Velthoven, P.: Trends and inter-annual variability of methane emissions derived from 1979-1993 global CTM simulations, *Atmos. Chem. Phys.*, 3, 73–88, doi:10.5194/acp-3-73-2003, 2003. 35421
- Dlugokencky, E. J., Myers, R. C., Lang, P. M., Masarie, K. A., Crotwell, A. M., Thoning, K. W., Hall, B. D., Elkins, J. W., and Steele, L. P.: Conversion of NOAA atmospheric dry air CH₄ mole fractions to a gravimetrically prepared standard scale, *J. Geophys. Res.-Atmos.*, 110, D18306, doi:10.1029/2005jd006035, 2005. 35424
- Emanuel, K. A. and Zivkovic-Rothman, M.: Development and evaluation of a convection scheme for use in climate models, *J. Atmos. Sci.*, 56, 1766–1782, doi:10.1175/1520-0469(1999)056<1766:DAEOAC>2.0.CO;2, 1999. 35427
- Empa: Technischer Bericht zum Nationalen Beobachtungsnetz für Luftfremdstoffe (NABEL) 2015, Tech. Rep. <http://www.empa.ch/web/s503/nabel>, Empa, available at: <http://www.empa.ch/documents/56101/246436/Nabel-technischer-bericht-15/>, last access: 14 December 2015. 35425
- Enting, I. G.: *Inverse Problems in Atmospheric Constituent Transport*, Cambridge University Press, 2002. 35421
- Eugster, W., DelSontro, T., and Sobek, S.: Eddy covariance flux measurements confirm extreme CH₄ emissions from a Swiss hydropower reservoir and resolve their short-term variability, *Biogeosciences*, 8, 2815–2831, doi:10.5194/bg-8-2815-2011, 2011. 35420
- Felber, R., Mürnger, A., Neftel, A., and Ammann, C.: Eddy covariance methane flux measurements over a grazed pasture: effect of cows as moving point sources, *Biogeosciences*, 12, 3925–3940, doi:10.5194/bg-12-3925-2015, 2015. 35456

Swiss methane emissions

S. Henne et al.

Title Page

Abstract

Introduction

Conclusions

References

Tables

Figures



Back

Close

Full Screen / Esc

Printer-friendly Version

Interactive Discussion



- FOEN: Switzerland's greenhouse gas inventory 1990–2012, Submission of April 2014 under the United Nations Framework Convention on Climate Change and under the Kyoto Protocol, Tech. rep., Federal Office for the Environment (FOEN), 2014. 35420, 35452, 35453, 35454
- 5 FOEN: Switzerland's greenhouse gas inventory 1990–2013, Submission of April 2015 under the United Nations Framework Convention on Climate Change and under the Kyoto Protocol, Tech. rep., Federal Office for the Environment (FOEN), 2015. 35420, 35422, 35436, 35452, 35454, 35455, 35459
- Forster, C., Stohl, A., and Seibert, P.: Parameterization of convective transport in a Lagrangian particle dispersion model and its evaluation, *J. Appl. Meteorol. Clim.*, 46, 403–422, doi:10.1175/JAM2470.1, 2007. 35427
- 10 Furger, M.: Die Radiosondierungen von Payerne: dynamisch-klimatologische Untersuchungen zur Vertikalstruktur des Windfeldes, Ph. D. thesis, University of Bern, zugl. Diss., Univ. Bern, 1990, 1990. 35439
- Gal-Chen, T. and Somerville, R. C. J.: On the use of a coordinate transformation for the solution of the Navier–Stokes equations, *Journal of Computational Physics*, 17, 209–228, doi:10.1016/0021-9991(75)90037-6, 1975. 35427
- 15 Gao, Z., Yuan, H., Ma, W., Li, J., Liu, X., and Desjardins, R. L.: Diurnal and Seasonal Patterns of Methane Emissions from a Dairy Operation in North China Plain, *Advances in Meteorology*, 2011, 190234, doi:10.1155/2011/190234, 2011. 35453
- 20 Gerbig, C., Körner, S., and Lin, J. C.: Vertical mixing in atmospheric tracer transport models: error characterization and propagation, *Atmos. Chem. Phys.*, 8, 591–602, doi:10.5194/acp-8-591-2008, 2008. 35433
- Hein, R., Crutzen, P. J., and Heimann, M.: An inverse modeling approach to investigate the global atmospheric methane cycle, *Global Biogeochem. Cy.*, 11, 43–76, doi:10.1029/96GB03043, 1997. 35421
- 25 Henne, S., Brunner, D., Folini, D., Solberg, S., Klausen, J., and Buchmann, B.: Assessment of parameters describing representativeness of air quality in-situ measurement sites, *Atmos. Chem. Phys.*, 10, 3561–3581, doi:10.5194/acp-10-3561-2010, 2010. 35424
- Hiller, R. V., Bretscher, D., DelSontro, T., Diem, T., Eugster, W., Henneberger, R., Hobi, S., Hodson, E., Imer, D., Kreuzer, M., Künzle, T., Merbold, L., Niklaus, P. A., Rihm, B., Schellenberger, A., Schroth, M. H., Schubert, C. J., Siegrist, H., Stieger, J., Buchmann, N., and Brunner, D.: Anthropogenic and natural methane fluxes in Switzerland synthesized within a
- 30

Swiss methane emissions

S. Henne et al.

Title Page

Abstract

Introduction

Conclusions

References

Tables

Figures



Back

Close

Full Screen / Esc

Printer-friendly Version

Interactive Discussion



spatially explicit inventory, *Biogeosciences*, 11, 1941–1959, doi:10.5194/bg-11-1941-2014, 2014a. 35419, 35420, 35422, 35436, 35447, 35455, 35456, 35457

Hiller, R. V., Neininger, B., Brunner, D., Gerbig, C., Bretscher, D., Künzle, T., Buchmann, N., and Eugster, W.: Aircraft-based CH₄ flux estimates for validation of emissions from an agriculturally dominated area in Switzerland, *J. Geophys. Res.-Atmos.*, 119, 4874–4887, doi:10.1002/2013JD020918, 2014b. 35420

Houweling, S., Kaminski, T., Dentener, F., Lelieveld, J., and Heimann, M.: Inverse modeling of methane sources and sinks using the adjoint of a global transport model, *J. Geophys. Res.-Atmos.*, 104, 26137–26160, doi:10.1029/1999JD900428, 1999. 35421

Hu, L., Montzka, S. A., Miller, J. B., Andrews, A. E., Lehman, S. J., Miller, B. R., Thoning, K., Sweeney, C., Chen, H., Godwin, D. S., Masarie, K., Bruhwiler, L., Fischer, M. L., Biraud, S. C., Torn, M. S., Mountain, M., Nehrkorn, T., Eluszkiewicz, J., Miller, S., Draxler, R. R., Stein, A. F., Hall, B. D., Elkins, J. W., and Tans, P. P.: U. S. emissions of HFC-134a derived for 2008–2012 from an extensive flask-air sampling network, *J. Geophys. Res.-Atmos.*, 120, 801–825, doi:10.1002/2014JD022617, 2015. 35451

IPCC: 2006 IPCC Guidelines for National Greenhouse Gas Inventories, available at: <http://www.ipcc-nggip.iges.or.jp/public/2006gl/index.html>, last access: 9 September 2015, 2006. 35420

JRC/PBL: Emission Database for Global Atmosphere Research (EDGAR), release version 4.0, Tech. rep., available at: <http://edgar.jrc.ec.europa.eu>, last access: 9 September 2015, 2009. 35436

Kirschke, S., Bousquet, P., Ciais, P., Saunois, M., Canadell, J. G., Dlugokencky, E. J., Bergamaschi, P., Bergmann, D., Blake, D. R., Bruhwiler, L., Cameron-Smith, P., Castaldi, S., Chevallier, F., Feng, L., Fraser, A., Heimann, M., Hodson, E. L., Houweling, S., Josse, B., Fraser, P. J., Krummel, P. B., Lamarque, J.-F., Langenfelds, R. L., Le Quere, C., Naik, V., O'Doherty, S., Palmer, P. I., Pison, I., Plummer, D., Poulter, B., Prinn, R. G., Rigby, M., Ringeval, B., Santini, M., Schmidt, M., Shindell, D. T., Simpson, I. J., Spahni, R., Steele, L. P., Strode, S. A., Sudo, K., Szopa, S., van der Werf, G. R., Voulgarakis, A., van Weele, M., Weiss, R. F., Williams, J. E., and Zeng, G.: Three decades of global methane sources and sinks, *Nat. Geosci.*, 6, 813–823, doi:10.1038/ngeo1955, 2013. 35419

Kort, E. A., Andrews, A. E., Dlugokencky, E., Sweeney, C., Hirsch, A., Eluszkiewicz, J., Nehrkorn, T., Michalak, A., Stephens, B., Gerbig, C., Miller, J. B., Kaplan, J., Houweling, S., Daube, B. C., Tans, P., and Wofsy, S. C.: Atmospheric constraints on 2004 emissions of methane and nitrous oxide in North America from atmospheric measurements and

Swiss methane emissions

S. Henne et al.

Title Page

Abstract

Introduction

Conclusions

References

Tables

Figures



Back

Close

Full Screen / Esc

Printer-friendly Version

Interactive Discussion



a receptor-oriented modeling framework, *Journal of Integrative Environmental Sciences*, 7, 125–133, doi:10.1080/19438151003767483, 2010. 35421

Kretschmer, R., Gerbig, C., Karstens, U., Biavati, G., Vermeulen, A., Vogel, F., Hammer, S., and Totsche, K. U.: Impact of optimized mixing heights on simulated regional atmospheric transport of CO₂, *Atmos. Chem. Phys.*, 14, 7149–7172, doi:10.5194/acp-14-7149-2014, 2014. 35425

Kuenen, J. J. P., Visschedijk, A. J. H., Jozwicka, M., and Denier van der Gon, H. A. C.: TNO-MACC_II emission inventory; a multi-year (2003–2009) consistent high-resolution European emission inventory for air quality modelling, *Atmos. Chem. Phys.*, 14, 10963–10976, doi:10.5194/acp-14-10963-2014, 2014. 35436

Manning, A. J., O'Doherty, S., Jones, A. R., Simmonds, P. G., and Derwent, R. G.: Estimating UK methane and nitrous oxide emissions from 1990 to 2007 using an inversion modeling approach, *J. Geophys. Res.-Atmos.*, 116, D02305, doi:10.1029/2010JD014763, 2011. 35421, 35442

McKain, K., Down, A., Raciti, S. M., Budney, J., Hutyra, L. R., Floerchinger, C., Herndon, S. C., Nehrkorn, T., Zahniser, M. S., Jackson, R. B., Phillips, N., and Wofsy, S. C.: Methane emissions from natural gas infrastructure and use in the urban region of Boston, Massachusetts, *P. Natl. Acad. Sci. USA*, 112, 1941–1946, doi:10.1073/pnas.1416261112, 2015. 35421, 35422, 35455, 35459

Meirink, J. F., Bergamaschi, P., and Krol, M. C.: Four-dimensional variational data assimilation for inverse modelling of atmospheric methane emissions: method and comparison with synthesis inversion, *Atmos. Chem. Phys.*, 8, 6341–6353, doi:10.5194/acp-8-6341-2008, 2008. 35421

Michalak, A. M., Hirsch, A., Bruhwiler, L., Gurney, K. R., Peters, W., and Tans, P. P.: Maximum likelihood estimation of covariance parameters for Bayesian atmospheric trace gas surface flux inversions, *J. Geophys. Res.-Atmos.*, 110, D24107, doi:10.1029/2005JD005970, 2005. 35435

Mikaloff Fletcher, S. E., Tans, P. P., Bruhwiler, L. M., Miller, J. B., and Heimann, M.: CH₄ sources estimated from atmospheric observations of CH₄ and its ¹³C/¹²C isotopic ratios: 2. Inverse modeling of CH₄ fluxes from geographical regions, *Global Biogeochem. Cy.*, 18, GB4005, doi:10.1029/2004GB002224, 2004. 35421

Miller, S. M., Wofsy, S. C., Michalak, A. M., Kort, E. A., Andrews, A. E., Biraud, S. C., Dlugokencky, E. J., Eluszkiewicz, J., Fischer, M. L., Janssens-Maenhout, G., Miller, B. R.,

Swiss methane emissions

S. Henne et al.

Title Page

Abstract

Introduction

Conclusions

References

Tables

Figures



Back

Close

Full Screen / Esc

Printer-friendly Version

Interactive Discussion



Miller, J. B., Montzka, S. A., Nehrkorn, T., and Sweeney, C.: Anthropogenic emissions of methane in the United States, *P. Natl. Acad. Sci. USA*, 110, 20018–20022, doi:10.1073/pnas.1314392110, 2013. 35421, 35454, 35459

5 Myhre, G., Shindell, D., Bréon, F., Collins, W., Fuglestvedt, J., Huang, J., Koch, D., Lamarque, J., Lee, D., Mendoza, B., Nakajima, T., Robock, A., Stephens, G., Takemura, T., and Zhang, H.: Anthropogenic and Natural Radiative Forcing, in: *Climate Change 2013: The Physical Science Basis. Contribution of Working Group I to the Fifth Assessment Report of the Intergovernmental Panel on Climate Change*, edited by: Stocker, T., Qin, D., Plattner, G., Tignor, M., Allen, S., Boschung, J., Nauels, A., Xia, Y., Bex, V., and Midgley, P., Cambridge University Press, Cambridge, UK and New York, NY, USA, 659–740, 2013. 35419

10 Nisbet, E. G., Dlugokencky, E. J., and Bousquet, P.: Methane on the Rise-Again, *Science*, 343, 493–495, doi:10.1126/science.1247828, 2014. 35419

Nocedal, J. and Wright, S. J.: *Numerical optimization*, Springer series in operation research and financial engineering, Springer-Verlag, New York, 2006. 35435

15 Oney, B., Henne, S., Gruber, N., Leuenberger, M., Bamberger, I., Eugster, W., and Brunner, D.: The CarboCount CH sites: characterization of a dense greenhouse gas observation network, *Atmos. Chem. Phys. Discuss.*, 15, 12911–12956, doi:10.5194/acpd-15-12911-2015, 2015. 35421, 35422, 35423, 35425, 35439

20 Pillai, D., Gerbig, C., Ahmadov, R., Rödenbeck, C., Kretschmer, R., Koch, T., Thompson, R., Neininger, B., and Lavrié, J. V.: High-resolution simulations of atmospheric CO₂ over complex terrain – representing the Ochsenkopf mountain tall tower, *Atmos. Chem. Phys.*, 11, 7445–7464, doi:10.5194/acp-11-7445-2011, 2011. 35426

Ramanathan, V. and Xu, Y.: The Copenhagen Accord for limiting global warming: criteria, constraints, and available avenues, *P. Natl. Acad. Sci. USA*, 107, 8055–8062, doi:10.1073/pnas.1002293107, 2010. 35419

25 Rella, C. W., Chen, H., Andrews, A. E., Filges, A., Gerbig, C., Hatakka, J., Karion, A., Miles, N. L., Richardson, S. J., Steinbacher, M., Sweeney, C., Wastine, B., and Zellweger, C.: High accuracy measurements of dry mole fractions of carbon dioxide and methane in humid air, *Atmos. Meas. Tech. Discuss.*, 5, 5823–5888, doi:10.5194/amtd-5-5823-2012, 2012. 35424

30 Rotach, M. W., Wohlfahrt, G., Hansel, A., Reif, M., Wagner, J., and Gohm, A.: The World is Not Flat: implications for the Global Carbon Balance, *B. Am. Meteorol. Soc.*, 95, 1021–1028, doi:10.1175/BAMS-D-13-00109.1, 2013. 35447

Swiss methane emissions

S. Henne et al.

Title Page

Abstract

Introduction

Conclusions

References

Tables

Figures



Back

Close

Full Screen / Esc

Printer-friendly Version

Interactive Discussion



- Ruckstuhl, A. F., Henne, S., Reimann, S., Steinbacher, M., Vollmer, M. K., O'Doherty, S., Buchmann, B., and Hueglin, C.: Robust extraction of baseline signal of atmospheric trace species using local regression, *Atmos. Meas. Tech.*, 5, 2613–2624, doi:10.5194/amt-5-2613-2012, 2012. 35425
- 5 Schmidt, M., Graul, R., Sartorius, H., and Levin, I.: Carbon dioxide and methane in continental Europe: a climatology, and 222 Radon-based emission estimates, *Tellus B*, 48, 457–473, doi:10.3402/tellusb.v48i4.15926, 1996. 35424
- Schneider, N. and Eugster, W.: Climatic impacts of historical wetland drainage in Switzerland, *Climatic Change*, 80, 301–321, doi:10.1007/s10584-006-9120-8, 2007. 35424
- 10 Schraff, C. H.: Mesoscale data assimilation and prediction of low stratus in the Alpine region, *Meteorol. Atmos. Phys.*, 64, 21–50, doi:10.1007/BF01044128, 1997. 35426
- Schroth, M. H., Eugster, W., Gómez, K. E., Gonzalez-Gil, G., Niklaus, P. A., and Oester, P.: Above- and below-ground methane fluxes and methanotrophic activity in a landfill-cover soil, *Waste Manage.*, 32, 879–889, doi:10.1016/j.wasman.2011.11.003, 2012. 35420
- 15 Schubert, C. J., Diem, T., and Eugster, W.: Methane Emissions from a Small Wind Shielded Lake Determined by Eddy Covariance, Flux Chambers, Anchored Funnels, and Boundary Model Calculations: a Comparison, *Environ. Sci. Technol.*, 46, 4515–4522, doi:10.1021/es203465x, 2012. 35420
- Shindell, D., Kuylenstierna, J. C. I., Vignati, E., van Dingenen, R., Amann, M., Klimont, Z., Anenberg, S. C., Muller, N., Janssens-Maenhout, G., Raes, F., Schwartz, J., Faluvegi, G., Pozzoli, L., Kupiainen, K., Höglund-Isaksson, L., Emberson, L., Streets, D., Ramanathan, V., Hicks, K., Oanh, N. T. K., Milly, G., Williams, M., Demkine, V., and Fowler, D.: Simultaneously Mitigating Near-Term Climate Change and Improving Human Health and Food Security, *Science*, 335, 183–189, doi:10.1126/science.1210026, 2012. 35419
- 20 Stieger, J., Bamberger, I., Buchmann, N., and Eugster, W.: Validation of farm-scale methane emissions using nocturnal boundary layer budgets, *Atmos. Chem. Phys. Discuss.*, 15, 21765–21802, doi:10.5194/acpd-15-21765-2015, 2015. 35420
- Stohl, A., Forster, C., Frank, A., Seibert, P., and Wotawa, G.: Technical note: The Lagrangian particle dispersion model FLEXPART version 6.2, *Atmos. Chem. Phys.*, 5, 2461–2474, doi:10.5194/acp-5-2461-2005, 2005. 35426
- 30 Stohl, A., Seibert, P., Arduini, J., Eckhardt, S., Fraser, P., Grealley, B. R., Lunder, C., Maione, M., Mühle, J., O'Doherty, S., Prinn, R. G., Reimann, S., Saito, T., Schmidbauer, N., Simmonds, P. G., Vollmer, M. K., Weiss, R. F., and Yokouchi, Y.: An analytical inversion method for

Swiss methane emissions

S. Henne et al.

Title Page

Abstract

Introduction

Conclusions

References

Tables

Figures



Back

Close

Full Screen / Esc

Printer-friendly Version

Interactive Discussion



determining regional and global emissions of greenhouse gases: Sensitivity studies and application to halocarbons, *Atmos. Chem. Phys.*, 9, 1597–1620, doi:10.5194/acp-9-1597-2009, 2009. 35429, 35432, 35436, 35446, 35448

Tarantola, A.: Inverse Problem Theory and Methods for Model Parameter Estimation, SIAM, Philadelphia, PA, 2005. 35430

Taylor, K. E.: Summarizing multiple aspects of model performance in a single diagram., *J. Geophys. Res.-Atmos.*, 106, 7183–7192, 2001. 35441

Thompson, R. L. and Stohl, A.: FLEXINVERT: an atmospheric Bayesian inversion framework for determining surface fluxes of trace species using an optimized grid, *Geosci. Model Dev.*, 7, 2223–2242, doi:10.5194/gmd-7-2223-2014, 2014. 35446

Thompson, R. L., Gerbig, C., and Rödenbeck, C.: A Bayesian inversion estimate of N₂O emissions for western and central Europe and the assessment of aggregation errors, *Atmos. Chem. Phys.*, 11, 3443–3458, doi:10.5194/acp-11-3443-2011, 2011. 35433

Thompson, R. L., Stohl, A., Zhou, L. X., Dlugokencky, E., Fukuyama, Y., Tohjima, Y., Kim, S. Y., Lee, H., Nisbet, E. G., Fisher, R. E., Lowry, D., Weiss, R. F., Prinn, R. G., O'Doherty, S., Young, D., and White, J. W. C.: Methane emissions in East Asia for 2000–2011 estimated using an atmospheric Bayesian inversion, *J. Geophys. Res.-Atmos.*, 120, 4352–4369, doi:10.1002/2014JD022394, 2015. 35442, 35446

Tiedtke, M.: A Comprehensive Mass Flux Scheme for Cumulus Parameterization in Large-Scale Models, *Mon. Weather Rev.*, 117, 1779–1800, doi:10.1175/1520-0493(1989)117<1779:ACMFSF>2.0.CO;2, 1989. 35427

Tolk, L. F., Meesters, A. G. C. A., Dolman, A. J., and Peters, W.: Modelling representation errors of atmospheric CO₂ mixing ratios at a regional scale, *Atmos. Chem. Phys.*, 8, 6587–6596, doi:10.5194/acp-8-6587-2008, 2008. 35426

Turner, A. J., Jacob, D. J., Wecht, K. J., Maasakkers, J. D., Lundgren, E., Andrews, A. E., Biraud, S. C., Boesch, H., Bowman, K. W., Deutscher, N. M., Dubey, M. K., Griffith, D. W. T., Hase, F., Kuze, A., Notholt, J., Ohyama, H., Parker, R., Payne, V. H., Sussmann, R., Sweeney, C., Velazco, V. A., Warneke, T., Wennberg, P. O., and Wunch, D.: Estimating global and North American methane emissions with high spatial resolution using GOSAT satellite data, *Atmos. Chem. Phys.*, 15, 7049–7069, doi:10.5194/acp-15-7049-2015, 2015. 35421, 35454, 35459

Swiss methane emissions

S. Henne et al.

[Title Page](#)[Abstract](#)[Introduction](#)[Conclusions](#)[References](#)[Tables](#)[Figures](#)[Back](#)[Close](#)[Full Screen / Esc](#)[Printer-friendly Version](#)[Interactive Discussion](#)

Tuzson, B., Hiller, R. V., Zeyer, K., Eugster, W., Neftel, A., Ammann, C., and Emmenegger, L.: Field intercomparison of two optical analyzers for CH₄ eddy covariance flux measurements, *Atmos. Meas. Tech.*, 3, 1519–1531, doi:10.5194/amt-3-1519-2010, 2010. 35420

Tuzson, B., Henne, S., Brunner, D., Steinbacher, M., Mohn, J., Buchmann, B., and Emmenegger, L.: Continuous isotopic composition measurements of tropospheric CO₂ at Jungfrauoch (3580 m a.s.l.), Switzerland: real-time observation of regional pollution events, *Atmos. Chem. Phys.*, 11, 1685–1696, doi:10.5194/acp-11-1685-2011, 2011. 35424

Vermeulen, A. T., Eisma, R., Hensen, A., and Slanina, J.: Transport model calculations of NW-European methane emissions, *Environ. Sci. Policy*, 2, 315–324, doi:10.1016/S1462-9011(99)00021-0, 1999. 35421

Wecht, K. J., Jacob, D. J., Frankenberg, C., Jiang, Z., and Blake, D. R.: Mapping of North American methane emissions with high spatial resolution by inversion of SCIAMACHY satellite data, *J. Geophys. Res.-Atmos.*, 119, 7741–7756, doi:10.1002/2014JD021551, 2014. 35421, 35454, 35459

Wennberg, P. O., Mui, W., Wunch, D., Kort, E. A., Blake, D. R., Atlas, E. L., Santoni, G. W., Wofsy, S. C., Diskin, G. S., Jeong, S., and Fischer, M. L.: On the Sources of Methane to the Los Angeles Atmosphere, *Environ. Sci. Technol.*, 46, 9282–9289, doi:10.1021/es301138y, 2012. 35421, 35455, 35459

Wüst-Galley, C., Grünig, A., and Leifeld, J.: Locating Organic Soils for the Swiss Greenhouse Gas Inventory, *Tech. rep.*, Agroscope, 2015. 35458

Zeitz, J. O., Soliva, C. R., and Kreuzer, M.: Swiss diet types for cattle: how accurately are they reflected by the Intergovernmental Panel on Climate Change default values?, *Journal of Integrative Environmental Sciences*, 9, 199–216, doi:10.1080/1943815X.2012.709253, 2012. 35453, 35454

Zellweger, C., Forrer, J., Hofer, P., Nyeki, S., Schwarzenbach, B., Weingartner, E., Ammann, M., and Baltensperger, U.: Partitioning of reactive nitrogen (NO_y) and dependence on meteorological conditions in the lower free troposphere, *Atmos. Chem. Phys.*, 3, 779–796, doi:10.5194/acp-3-779-2003, 2003. 35424

Swiss methane emissions

S. Henne et al.

Title Page

Abstract

Introduction

Conclusions

References

Tables

Figures



Back

Close

Full Screen / Esc

Printer-friendly Version

Interactive Discussion

**Table 1.** Overview of the location of the observational sites used in the study, including particle release heights as used in FLEXPART simulations. See text for details on release height selection.

Station	ID	Longitude (° E)	Latitude (° N)	Altitude (m a.s.l.)	COSMO-7 height (m a.s.l.)	Inlet height (m)	low release (m)	high release (m)
Beromünster	BEO	8.1755	47.1896	797	615	212	212 a.g.l.	1014 a.s.l.
Lägern Hochwacht	LAE	8.3973	47.4822	840	492	32	150 a.g.l.	250 a.g.l.
Schauinsland	SSL	7.9167	47.9000	1205	750	10	980 a.s.l.	–
Jungfrauojoch	JFJ	7.9851	46.5475	3580	2650	3	3100 a.s.l.	–
Früebüel	FRU	8.5378	47.1158	982	711	5	50 a.g.l.	982 a.s.l.
Gimmiz	GIM	7.2480	47.0536	443	496	32	32 a.g.l.	–

Swiss methane emissions

S. Henne et al.

Table 2. Setup of the base (B) and sensitivity inversions (S-X).

Inversion	Method	FLEXPART version	Sites	Baseline method	Seasonality	Prior emissions	Model/Observation uncertainty
B	Bayesian	COSMO	BEO, LAE, JFJ, SSL	Single	N	MAIOLICA	standard
S-V	Bayesian	COSMO	BEO, LAE, JFJ, SSL	Single	Y	MAIOLICA	standard
S-K	extKF	COSMO	BEO, LAE, JFJ, SSL	Single	Y	MAIOLICA	standard
S-EC	Bayesian	ECMWF	BEO, LAE, JFJ, SSL	Single	N	MAIOLICA	standard
S-T	Bayesian	COSMO	BEO, LAE, JFJ, SSL	Single	N	TNO/MACC-2	standard
S-E	Bayesian	COSMO	BEO, LAE, JFJ, SSL	Single	N	EDGAR	standard
S-S	Bayesian	COSMO	BEO, LAE, JFJ, SSL	Single	N	MAIOLICA	Stohl
S-ML	Bayesian	COSMO	BEO, LAE, JFJ, SSL	Single	N	MAIOLICA	ML
S-O1	Bayesian	COSMO	BEO	Single	N	MAIOLICA	standard
S-O2	Bayesian	COSMO	LAE	Single	N	MAIOLICA	standard
S-O3	Bayesian	COSMO	BEO LAE	Single	N	MAIOLICA	standard
S-O4	Bayesian	COSMO	BEO, LAE, JFJ, SSL, FRU	Single	N	MAIOLICA	standard
S-O5	Bayesian	COSMO	BEO, LAE, JFJ, SSL, FRU, GIM	Single	N	MAIOLICA	standard
S-B1	Bayesian	COSMO	BEO, LAE, JFJ, SSL	Gradient	N	MAIOLICA	standard
S-B2	Bayesian	COSMO	BEO, LAE, JFJ, SSL	Grid	N	MAIOLICA	standard

Title Page

Abstract

Introduction

Conclusions

References

Tables

Figures



Back

Close

Full Screen / Esc

Printer-friendly Version

Interactive Discussion



Swiss methane emissions

S. Henne et al.

Table 3. Overview of parameters used for the construction of the uncertainty covariance matrices: contributions to model/observation uncertainty σ_{\min} and σ_{srr} , baseline uncertainty factor f_b , baseline correlation length τ_b , prior correlation length L and prior Swiss emission uncertainty σ_E .

	σ_{\min} (nmol mol ⁻¹)				σ_{srr} (-)				f_b (-)			τ_b (d)	L (km)	σ_E (%)	
	BEO	LAE	SSL	JFJ	BEO	LAE	SSL	JFJ	BEO	LAE	SSL				JFJ
Base inversion (B-B)															
low	11	16	11	17	0.53	0.47	0.34	0.36	1	1	1	1	14	50	16
high	22	23	11	17	0.45	0.46	0.35	0.36	1	1	1	1	14	50	16
Stohl09 (S-S)															
low	40	41	22	20	0	0	0	0	1	1	1	1	14	50	16
high	41	44	22	20	0	0	0	0	1	1	1	1	14	50	16
Maximum likelihood (S-ML)															
low	25	24	19	20	0.78	0.76	0.54	1.24	3.6	5.1	2.1	2.0	19	50	31
high	39	35	19	20	0.64	0.63	0.54	1.23	4.2	5.5	2.4	2.4	23	51	30
Extended Kalman Filter (S-K)															
low	14	14	14	14	0.5	0.5	0.5	0.5	–	–	–	–	–	50	16
high	14	14	14	14	0.5	0.5	0.5	0.5	–	–	–	–	–	50	16



Table 4. Overview of results of sensitivity inversions. E_A and E_B are the total Swiss CH₄ prior and posterior emissions (Ggyr⁻¹), respectively, and S is the posterior Taylor skill score for the individual sites. The settings of the sensitivity inversions are given in Table 2.

Inversion	Emissions		Skill score (S)					
	prior E_A	posterior E_B	BEO	LAE	SSL	JFJ	FRU	GIM
B low	183.0 ± 29.3	179.0 ± 7.0	0.83	0.89	0.91	0.78	0.77	0.50
B high	183.0 ± 29.3	195.0 ± 7.3	0.84	0.86	0.91	0.78	0.74	0.51
S-V low	183.0 ± 29.3	185.9 ± 6.5	0.84	0.89	0.91	0.77	0.77	0.51
S-V high	183.0 ± 29.3	197.3 ± 6.7	0.85	0.86	0.91	0.78	0.75	0.53
S-K low	179.6 ± 28.7	193.1 ± 13	0.92	0.94	0.94	0.84	–	–
S-K high	179.6 ± 28.7	216.7 ± 14	0.93	0.95	0.94	0.85	–	–
S-EC low	184.4 ± 28.0	171.1 ± 8.0	0.79	0.87	0.91	0.77	0.74	0.29
S-EC high	184.5 ± 29.0	182.1 ± 7.6	0.88	0.87	0.92	0.77	0.74	0.31
S-T low	188.1 ± 30.1	180.3 ± 7.2	0.82	0.89	0.91	0.78	0.74	0.44
S-T high	187.7 ± 29.7	199.1 ± 7.4	0.83	0.87	0.91	0.78	0.69	0.46
S-E low	228.2 ± 36.5	184.3 ± 7.9	0.84	0.89	0.90	0.77	0.75	0.43
S-E high	227.4 ± 36.4	207.1 ± 7.9	0.83	0.88	0.90	0.77	0.69	0.46
S-S low	183.3 ± 29.3	169.3 ± 7.5	0.79	0.84	0.89	0.77	0.70	0.39
S-S high	183.3 ± 29.3	197.6 ± 8.0	0.81	0.84	0.89	0.77	0.70	0.51
S-ML low	183.0 ± 37.3	158.4 ± 13	0.84	0.92	0.90	0.78	0.73	0.44
S-ML high	183.0 ± 65.6	168.7 ± 13	0.85	0.91	0.89	0.78	0.66	0.44
S-O1 low	184.9 ± 29.2	183.3 ± 10	0.85	0.83	0.84	0.62	0.78	0.40
S-O1 high	184.6 ± 29.5	200.8 ± 11	0.87	0.81	0.84	0.63	0.78	0.38
S-O2 low	185.8 ± 29.7	214.3 ± 11	0.77	0.90	0.83	0.66	0.77	0.57
S-O2 high	184.5 ± 29.6	229.6 ± 11	0.75	0.88	0.82	0.66	0.76	0.64
S-O3 low	183.3 ± 29.3	198.5 ± 7.9	0.85	0.91	0.84	0.66	0.79	0.49
S-O3 high	183.5 ± 29.4	221.3 ± 8.3	0.86	0.89	0.83	0.66	0.78	0.51
S-O4 low	183.3 ± 28.3	191.2 ± 6.2	0.84	0.90	0.91	0.78	0.82	0.46
S-O4 high	183.3 ± 29.2	207.7 ± 6.5	0.85	0.88	0.91	0.79	0.85	0.48
S-O5 low	181.9 ± 29.1	208.8 ± 6.0	0.84	0.90	0.92	0.79	0.83	0.66
S-O5 high	181.9 ± 29.1	224.3 ± 6.1	0.85	0.88	0.91	0.79	0.85	0.69
S-B1 low	183.0 ± 29.3	194.0 ± 6.9	0.83	0.89	0.92	0.79	0.77	0.49
S-B1 high	183.0 ± 29.3	211.7 ± 7.2	0.84	0.87	0.92	0.79	0.74	0.51
S-B2 low	183.0 ± 29.3	195.1 ± 6.9	0.88	0.89	0.92	0.83	0.82	0.62
S-B2 high	183.0 ± 29.3	223.6 ± 6.9	0.88	0.88	0.92	0.83	0.75	0.69

Swiss methane emissions

S. Henne et al.

Title Page

Abstract

Introduction

Conclusions

References

Tables

Figures

◀

▶

◀

▶

Back

Close

Full Screen / Esc

Printer-friendly Version

Interactive Discussion



Swiss methane emissions

S. Henne et al.

Title Page

Abstract

Introduction

Conclusions

References

Tables

Figures

I◀

▶I

◀

▶

Back

Close

Full Screen / Esc

Printer-friendly Version

Interactive Discussion



Table 5. Swiss CH₄ emissions (Ggyr⁻¹) by most relevant source process as reported to UN-FCCC for the year 2012 and total emissions as estimated by this study. Uncertainties denote 1σ confidence levels.

Source	FOEN 2014	FOEN 2015	This study
Total	176 ± 28	206 ± 33	197 ± 19
1A Fuel combustion	4.1	3.7	
1B Fugitive emissions from fuels	8.1	8.4	
2 Industrial processes	0.1	0.1	
3A Enteric fermentation	118.9	130.5	
3B Manure management	30.8	31.0	
5A Solid waste disposal on land	7.5	8.5	
5B Biological treatment of waste ^a	5.4	16.7	
5C Waste incineration ^b	0.3	0.3	
5D Waste water handling	0.4	6.8	

^a composting and anaerobic digestion.

^b without municipal solid waste incineration.

Swiss methane emissions

S. Henne et al.

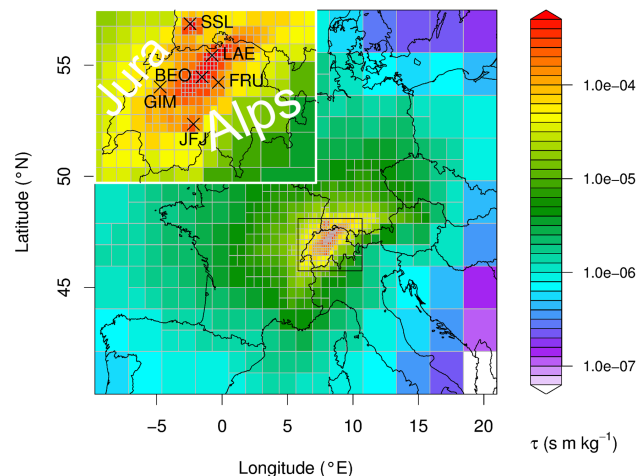


Figure 1. Total source sensitivity for the period March 2013 to February 2014 and the 4 sites used in the base inversion (crosses and labels in subplot; BEO: Beromünster, LAE: Lägern, JFJ: Jungfrauoch, SSL: Schauinsland). Source sensitivities are displayed on the reduced resolution grid that is used in the inversion. The units of the source sensitivity are given as residence times divided by atmospheric density and surface area. The locations of the two validation sites (FRU: Frübüel and GIM: Gimmiz) are given in the subplot as well.

Title Page

Abstract

Introduction

Conclusions

References

Tables

Figures

◀

▶

◀

▶

Back

Close

Full Screen / Esc

Printer-friendly Version

Interactive Discussion



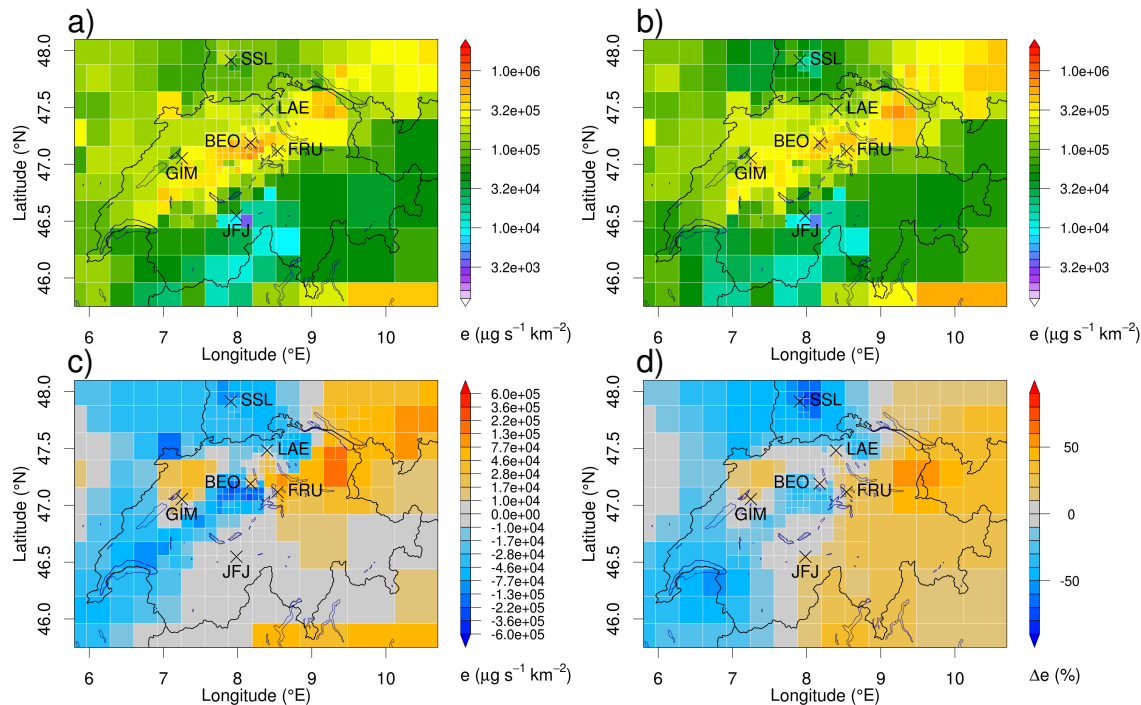


Figure 2. (a) prior and (b) posterior surface fluxes of CH_4 in the base inversion and low particle release heights (B low). (c) absolute and (d) relative (to prior) difference between posterior and prior emission fluxes. For panels c and d red (blue) colors indicate higher (lower) posterior than prior emissions.

Title Page

Abstract

Introduction

Conclusions

References

Tables

Figures

◀

▶

◀

▶

Back

Close

Full Screen / Esc

Printer-friendly Version

Interactive Discussion



Swiss methane emissions

S. Henne et al.

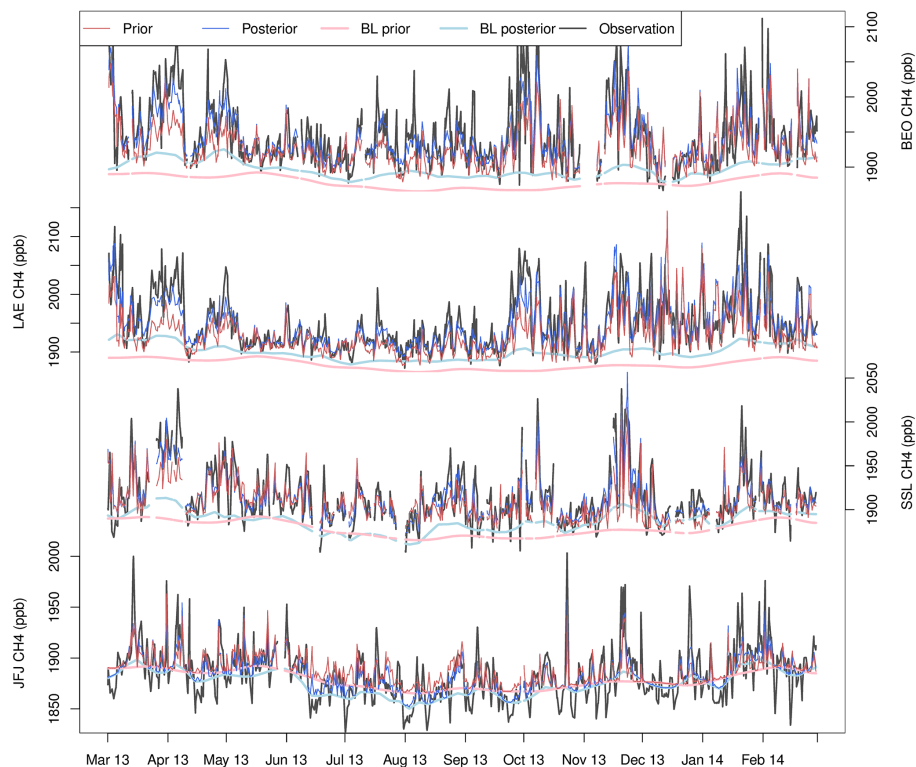


Figure 3. Observed (black) and simulated (prior: red; posterior: blue) CH_4 time series in the base inversion with low release heights (B low) at sites used in the inversion. Also given are the baseline mole fractions as used in the simulations (prior: light red; posterior: light blue). Note that the y axes were scaled for each site separately.

[Title Page](#)[Abstract](#)[Introduction](#)[Conclusions](#)[References](#)[Tables](#)[Figures](#)[Back](#)[Close](#)[Full Screen / Esc](#)[Printer-friendly Version](#)[Interactive Discussion](#)

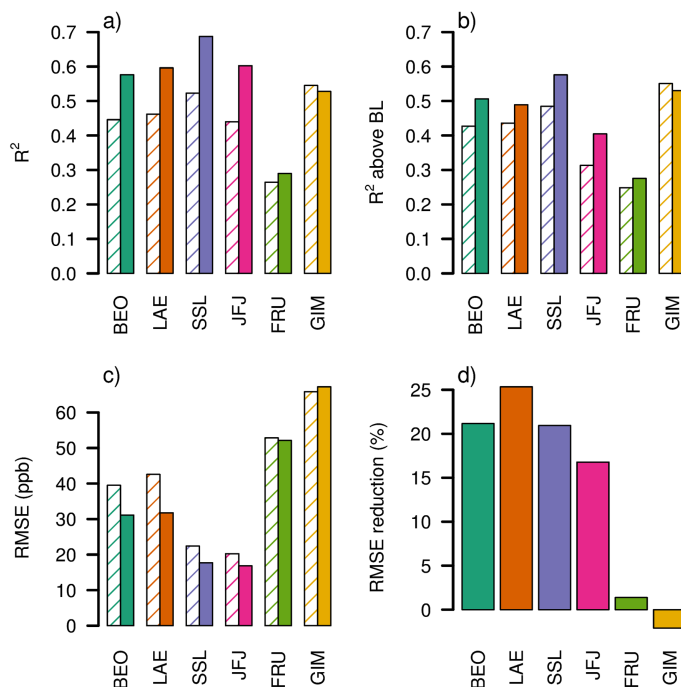


Figure 4. Model performance parameters for simulated time series at all sites for the base inversion with low particle release heights (B low): prior (shaded) and posterior (filled). **(a)** coefficient of determination (R^2) for complete signal and **(b)** above baseline signal, **(c)** normalised RMSE and **(d)** reduction of RMSE between prior and posterior. Note that the FRU and GIM sites were only used for validation but not in the inversion.

Swiss methane emissions

S. Henne et al.

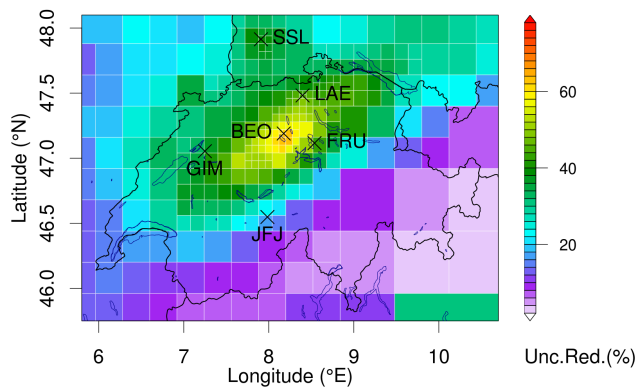


Figure 5. Uncertainty reduction between prior and posterior fluxes given in % relative to prior uncertainty ($1 - \sigma_B/\sigma_A$) for the base inversion with low particle release height.

[Title Page](#)[Abstract](#)[Introduction](#)[Conclusions](#)[References](#)[Tables](#)[Figures](#)[◀](#)[▶](#)[◀](#)[▶](#)[Back](#)[Close](#)[Full Screen / Esc](#)[Printer-friendly Version](#)[Interactive Discussion](#)

Swiss methane emissions

S. Henne et al.

Title Page

Abstract

Introduction

Conclusions

References

Tables

Figures



Back

Close

Full Screen / Esc

Printer-friendly Version

Interactive Discussion

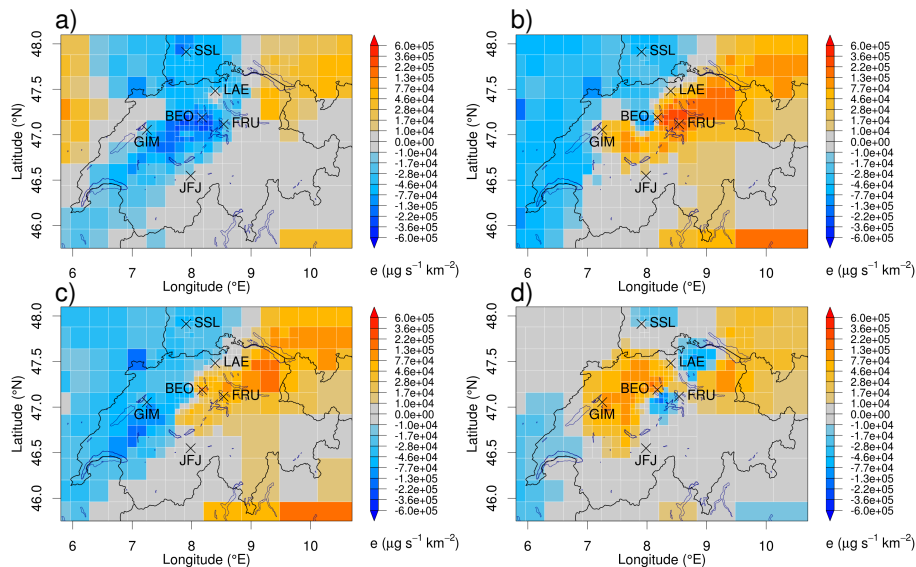


Figure 6. Absolute difference between posterior minus prior emission fluxes for seasonal inversion. **(a)** December, January, February, **(b)** March, April, May, **(c)** June, July, August, **(d)** September, October, November.

Swiss methane emissions

S. Henne et al.

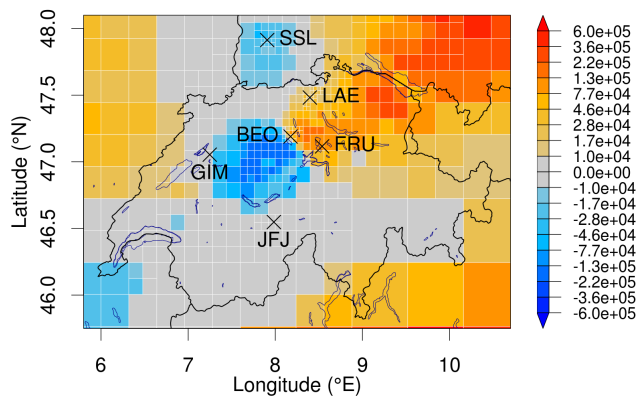


Figure 7. Absolute difference between posterior minus prior emission fluxes as obtained from extended Kalman filter inversion with low particle releases.

[Title Page](#)[Abstract](#)[Introduction](#)[Conclusions](#)[References](#)[Tables](#)[Figures](#)[Back](#)[Close](#)[Full Screen / Esc](#)[Printer-friendly Version](#)[Interactive Discussion](#)

Swiss methane emissions

S. Henne et al.

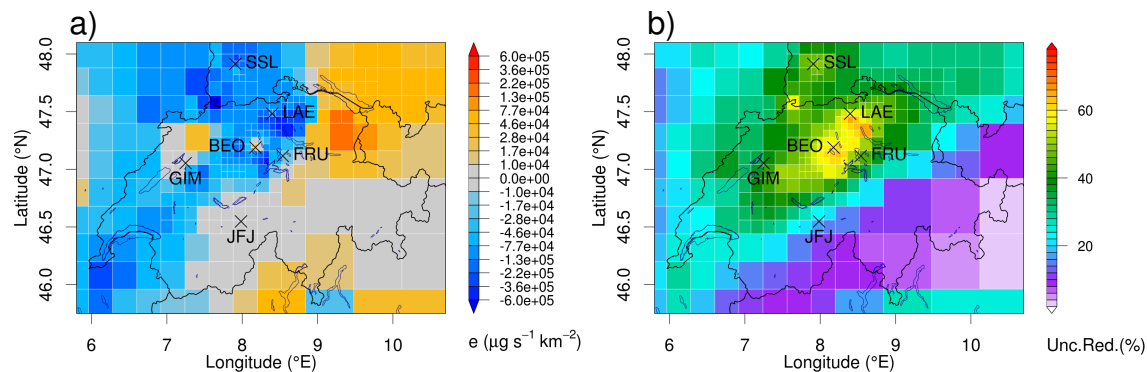


Figure 9. Absolute difference between posterior minus prior emission fluxes when using EDGAR instead of MAIOLICA prior fluxes.

Title Page

Abstract

Introduction

Conclusions

References

Tables

Figures

◀

▶

◀

▶

Back

Close

Full Screen / Esc

Printer-friendly Version

Interactive Discussion



Swiss methane emissions

S. Henne et al.

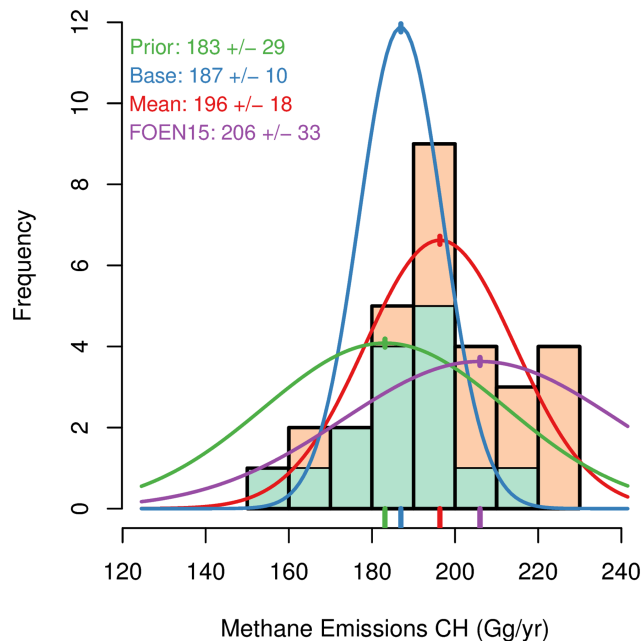


Figure 10. Histogram of total Swiss CH₄ emissions taken from all individual sensitivity inversions: low (light green) and high (light orange) particle releases. The base inversion prior (green) and posterior (blue) estimate as well as the average over all sensitivity inversions (red) and the FOEN2015 estimate (purple) are indicated by their Gaussian probability density functions.

[Title Page](#)[Abstract](#)[Introduction](#)[Conclusions](#)[References](#)[Tables](#)[Figures](#)[◀](#)[▶](#)[◀](#)[▶](#)[Back](#)[Close](#)[Full Screen / Esc](#)[Printer-friendly Version](#)[Interactive Discussion](#)